




2017

ANALYSIS AND SIMULATION OF PHOTOVOLTAIC SYSTEMS INCORPORATING BATTERY ENERGY STORAGE

Oluwaseun M. Akeyo

University of Kentucky, ochichikeyo@gmail.com

Author ORCID Identifier:

 <https://orcid.org/0000-0002-2862-9527>

Digital Object Identifier: <https://doi.org/10.13023/ETD.2017.370>

[Right click to open a feedback form in a new tab to let us know how this document benefits you.](#)

Recommended Citation

Akeyo, Oluwaseun M., "ANALYSIS AND SIMULATION OF PHOTOVOLTAIC SYSTEMS INCORPORATING BATTERY ENERGY STORAGE" (2017). *Theses and Dissertations--Electrical and Computer Engineering*. 107.

https://uknowledge.uky.edu/ece_etds/107

This Master's Thesis is brought to you for free and open access by the Electrical and Computer Engineering at UKnowledge. It has been accepted for inclusion in Theses and Dissertations--Electrical and Computer Engineering by an authorized administrator of UKnowledge. For more information, please contact UKnowledge@lsv.uky.edu.

STUDENT AGREEMENT:

I represent that my thesis or dissertation and abstract are my original work. Proper attribution has been given to all outside sources. I understand that I am solely responsible for obtaining any needed copyright permissions. I have obtained needed written permission statement(s) from the owner(s) of each third-party copyrighted matter to be included in my work, allowing electronic distribution (if such use is not permitted by the fair use doctrine) which will be submitted to UKnowledge as Additional File.

I hereby grant to The University of Kentucky and its agents the irrevocable, non-exclusive, and royalty-free license to archive and make accessible my work in whole or in part in all forms of media, now or hereafter known. I agree that the document mentioned above may be made available immediately for worldwide access unless an embargo applies.

I retain all other ownership rights to the copyright of my work. I also retain the right to use in future works (such as articles or books) all or part of my work. I understand that I am free to register the copyright to my work.

REVIEW, APPROVAL AND ACCEPTANCE

The document mentioned above has been reviewed and accepted by the student's advisor, on behalf of the advisory committee, and by the Director of Graduate Studies (DGS), on behalf of the program; we verify that this is the final, approved version of the student's thesis including all changes required by the advisory committee. The undersigned agree to abide by the statements above.

Oluwaseun M. Akeyo, Student

Dr. Dan M. Ionel, Major Professor

Dr. Caicheng Lu, Director of Graduate Studies

ANALYSIS AND SIMULATION OF PHOTOVOLTAIC SYSTEMS
INCORPORATING BATTERY ENERGY STORAGE

THESIS

A thesis submitted in partial fulfillment
of the requirements for the degree of
Master of Science in Electrical
Engineering in the College of Engineering
at the University of Kentucky

By

Oluwaseun Akeyo
Lexington, Kentucky

Director: Dr. Dan M. Ionel, Professor and L. Stanley Pigman Chair in Power
Lexington, Kentucky 2017

Copyright© Oluwaseun Akeyo 2017

ABSTRACT OF THESIS

ANALYSIS AND SIMULATION OF PHOTOVOLTAIC SYSTEMS
INCORPORATING BATTERY ENERGY STORAGE

Solar energy is an abundant renewable source, which is expected to play an increasing role in the grid's future infrastructure for distributed generation. The research described in the thesis focuses on the analysis of integrating multi-megawatt photovoltaics systems with battery energy storage into the existing grid and on the theory supporting the electrical operation of components and systems. The PV system is divided into several sections, each having its own DC-DC converter for maximum power point tracking and a two-level grid connected inverter with different control strategies. The functions of the battery are explored by connecting it to the system in order to prevent possible voltage fluctuations and as a buffer storage in order to eliminate the power mismatch between PV array generation and load demand. Computer models of the system are developed and implemented using the *PSCADTM/EMTDCTM* software.

KEYWORDS: photovoltaics, battery, energy storage, inverter, solar pump, IEEE 14 bus.

Author's signature: Oluwaseun Akeyo

Date: July 31, 2017

ANALYSIS AND SIMULATION OF PHOTOVOLTAIC SYSTEMS
INCORPORATING BATTERY ENERGY STORAGE

By
Oluwaseun Akeyo

Director of Thesis: Dr. Dan M. Ionel

Director of Graduate Studies: Dr. Caicheng Lu

Date: July 31, 2017

DEDICATION

*Dedicated to my parents
for their infinite love, support, and encouragement*

ACKNOWLEDGEMENTS

First of all, I would like to express my profound gratitude to my supervisor Dr. Dan. M. Ionel for his guidance, mentoring, constant encouragement and selfless support throughout this research. I also wish to thank him for giving me the opportunity to serve as a research assistant in the SPARK Laboratory, University of Kentucky. I am deeply indebted to Dr. Vandana Rallabandi, who always made time to assist me with my simulations and guided me through the fundamentals of research.

I am also grateful to Dr. Aaron M. Cramer and Dr. Yuan Liao for their review and input as members of my thesis committee. Special thanks are due to the team of experts at Nayak Corp. led by Dr. Om Nayak for their expert advice on the PSCAD simulation software. The support of University of Kentucky, electrical and computer engineering department and the L. Stanley Pigman endowment are gratefully acknowledged.

I would also like to thank my parents for their endless support and for allowing me realize my own potential. Without you, I would not be able to be who I am today.

Last but not the least, I would like to say a huge thanks to my fiancée, Miss Oretha Shannon who was understanding and there for me throughout this thesis and also my colleagues and friends at SPARK Lab, with whom it has been wonderful to work with.

Oluwaseun Akeyo
August, 2017

Contents

ACKNOWLEDGEMENTS	iii
List of Figures	vii
List of Tables	xiii
1 Introduction	1
1.1 Research Background	2
1.2 Thesis Outline	4
2 Conceptual Developments	5
2.1 Introduction	5
2.2 Photovoltaic Cells and Arrays	6
2.2.1 PV cell output characteristics	9
2.2.2 PV module and array setup	13
2.2.3 Maximum power point tracking	16
2.3 Power Electronics Converters and Electric Machines	18
2.3.1 DC/DC converters	19
2.3.2 AC/DC converters	22
2.3.3 Electric machines for pump systems	27
2.4 Battery Energy Storage Systems (BESS)	32
2.4.1 BESS management	32

2.4.2	BESS interface	34
2.5	Summary	35
3	Integrating PV and Energy Storage Connected to the IEEE 14 Bus Modified Test System	36
3.1	Introduction	36
3.2	PV System	39
3.2.1	PV array	39
3.2.2	MPPT	42
3.3	Grid-Connected Inverter	43
3.4	BESS	45
3.5	Modified IEEE 14 Bus Test System	47
3.6	Simulation Results and Discussion	51
3.7	Summary	56
4	Solar PV Pumping System with Capacity Modulation and Battery Voltage Support	60
4.1	Introduction	60
4.2	System Configuration	62
4.2.1	PV array	64
4.2.2	BESS	64
4.2.3	Pump system	65
4.3	Design Considerations	66
4.4	Proposed System Control	67
4.4.1	DC-DC converters	67
4.4.2	DC-AC converters	68
4.4.3	Capacity modulation	70
4.5	Simulation Results and Discussion	71

4.6	Summary	77
5	Conclusions and Future Work	82
5.1	Conclusions	82
5.2	Future Work	83
	References	86
	Curriculum Vitae	99

List of Figures

2.1	Irradiance variation for a full day, with example data sampled every 5min collected from the roof of RGAN building at University of Kentucky on a (a) clear and, (b) cloudy day [1].	7
2.2	Equivalent circuit diagram of PV cell (a) ideal and, (b) real.	8
2.3	(a) Setup in PSCAD environment for a simple PV circuit with variable output voltage, and (b) PV cell properties dialog box in PSCAD. . .	11
2.4	The cell output voltage and maximum power increases with decrease in cell temperature at constant $1000\text{W}/\text{m}^2$ solar irradiance (a) I-V curve, (b) P-V curve. Cell output voltage increases with increase in solar irradiance at constant 25°C cell temperature (c) I-V curve, (d) P-V curve.	12
2.5	(a) Solar PV cell configuration from solar cell to solar array [2], (b) IV curve of solar PVs with different configurations [3].	14
2.6	Schematic diagram in PSCAD/EMTDC for DC/DC converter (a) buck, (b) boost , (c) buck-boost and (d) Ćuk	20
2.7	Input and output voltage result in PSCAD/EMTDC with duty cycle changing from 0.3 to 0.8 at 0.5secs simulation time for DC/DC converter (a) boost, (b) buck , (c) buck-boost and (d) Ćuk	21
2.8	Circuit diagram for a full bridge uncontrolled diode rectifier.	23
2.9	Circuit diagram for a 3-phase voltage source inverter	26

2.10	Steady state torque-speed curve for a typical induction motor (T_e) and a pump load (T_1). The operating point is at the intersection of the two curves (A or B) [4].	28
2.11	Block diagram of V/f control structure with stator frequency reference input	30
2.12	Block diagram of vector control for PMSM [5]	31
2.13	(a) Non- isolated half-bridge DC/DC converter, (b) voltage-fed isolated DC/DC converter [6].	34
3.1	Schematic of a grid tied solar PV system consisting of several units in parallel with individual transformer connected to the grid for generality since design can also be implemented with a single transformer. The battery energy storage system is connected to the grid through its own inverter and transformer as well.	38
3.2	Power circuit diagram in PSCAD simulator showing the solar PV panel, DC-DC converter, 2-level inverter, transformer and grid. Practical implementations may use a Δ -Y transformer also.	40
3.3	I-V characteristic of PV array at 25° and $1000\text{W}/\text{m}^2$ solar irradiance. For maximum output power, it is recommended to operate the PV at the knee of the curve.	41
3.4	Control diagram for DC-DC converter using blocks from the PSCAD library.	43
3.5	Schematic diagram of proposed 3-level inverter formed by cascading two 2-level PV inverters. More levels may be obtained by cascading more inverters in the system.	44

3.6	Grid side inverter control diagram. The control maintains I_d at zero so that the inverter neither absorbs nor supply reactive power while I_q is used to regulate the real power output by keeping the bus voltage constant at a reference value.	45
3.7	Control diagram for BESS reference current components. $I_{qbre f}$ and I_{dbref} are fed to an inner controller to generate voltage reference, which is subsequently used to produce inverter gating signals.	47
3.8	Modified IEEE 14 bus system considered in the current study with the PV source supplying part of the power at bus no. 2.	49
3.9	PV DC Power. Reduction in irradiance leads to decrease in PV output current making the PV DC power alternate with respect to changes in irradiance.	52
3.10	PV AC power output at unity power factor irrespective of changes in array irradiance.	52
3.11	PV array MPPT reference and terminal voltage. With changes in irradiance, DC-DC converter ensures that the PV array still operates at MPPT.	53
3.12	The control loop maintains the DC link voltage at 0.6kV by regulating the q-axis current component.	53
3.13	Inverter actual and reference current components. I_d^* is maintained at 0 so that reactive current component is zero and I_q^* is regulated to maintain the PV DC bus voltage at reference value	54
3.14	BESS real power output. At 1000W/m ² the PV system is supplying excess power allowing the BESS to charge, when array is suddenly shaded, BESS changes from charging to discharging mode to supply the power deficit.	54

3.15 (a) Inverter input current and, (b) zoomed representation. The inverter input current is discontinuous due to high frequency switching of inverter switches and its maximum current reduces with decrease in the amount of PV irradiance	55
3.16 (a) PV system output current and, (b) zoomed representation . When PV array irradiance reduces, I_q^* reduces so that DC link voltage is maintained at reference value.	55
3.17 Grid voltage. Grid voltage is maintained constant with changes in PV irradiance.	56
3.18 PV system and synchronous generator real power output ($S_{base} = 100\text{MW}$). Adjacent synchronous generator increases its turbine mechanical power to supply power lost from PV.	57
3.19 Generator output current increases when PV is being shaded to supply the power deficit.	57
3.20 Modified IEEE 14 bus no 2 frequency. The sudden loss of PV power leads to a transient in the bus voltage frequency before the generator power increases to supply the power deficit and maintain the frequency at 60Hz.	58
3.21 Bus no 2 RMS voltage. The bus voltage is maintained within acceptable limit throughout the transient ($V_{base} = 138\text{kV}$).	58
4.1 System overview showing how existing pumping system connected to the grid can be expanded with multiple PMSM driven pumps for capacity modulation powered by solar PV. The grid in this system is used to maintain DC bus when battery is unavailable due to SOC constraints and $V(\text{mmpt})$ is the MPPT voltage at $1000\text{W}/\text{m}^2$ with 25°C cell temperature	63

4.2	(a) BESS connected to the DC bus through DC-DC converter where switch S1 is used to regulate the charge current and S2 controls the discharge current, (b) BESS converter control so that battery supplies the amount of current required to keep DC link voltage at reference value	69
4.3	PMSM inverter control	70
4.4	Capacity modulation control	71
4.5	PV array DC output power. PV array operates at MPP until battery switches from charging to discharging mode at 40s leading to transient in MPPT computation.	72
4.6	DC bus voltage. At 40s simulation time, power required to energize the pump at reference speed is greater than power from the PV array, which lead to drop in bus voltage before the battery starts to discharge.	73
4.7	Battery output current. Battery absorbs the excess energy from the PV array to maintain the DC link bus voltage at 1kV and supplies power to the DC link at 40s when the bus voltage is below reference.	73
4.8	Pump torque. With increase in PV reference speed, PMSM torque increases corresponding to the square of the reference speed	74
4.9	Pump reactive and real power intake. The single PMSM pump connected to the system is rated for 0.8MVA and absorbs real and reactive power sufficient to keep it operating at the reference speed with maximum torque.	74
4.10	PMSM speed. With increase in load demand, PMSM inverter adjust to increase the pump speed	75
4.11	MPPT reference and PV array output voltage. At 40s when the battery changers from discharging to charging mode, the MPPT adjust its reference so the PV remains at its MPP	75

4.12	Pump inverter reference active current component. In order to increase the pump speed, the reference active current component (I_q^*) is also increase.	76
4.13	(a) Pump current and, (b) zoomed representation. With increase in speed reference, the pump absorbs more current to meet the load demand.	76
4.14	Reference MPPT and PV array output voltage when irradiance suddenly drops from 1000W/m ² to 500W/m ² at 7s simulation time for 8s making the duty cycle of the DC-DC converter change so that the PV sees a load corresponding to its new maximum power.	78
4.15	Battery output current with change in irradiance effect when the PMSM driven pumps are modulated for 80% load. Irradiance change causes the battery to switch from charging to discharging to supply deficit power required to keep the pumps operating at reference speed. . . .	78
4.16	DC output power from PV array. When PV array is suddenly shaded, transient effect makes the array slightly move away from its MPP for a short period of time before settling at a new MPP corresponding to the level of solar irradiance.	79
4.17	Pump speed when reference load changes from 25% to 50%, 75%, 80% and 100% at 10s, 20s, 30s and 40s simulation time respectively making the amount of energized pumps increase to meet speed demand. . . .	79
4.18	Pump electrical torque, which is proportional to the square of the operating speed of each pump.	80
4.19	DC link and reference voltage. BESS charges and discharge to maintain DC link voltage at reference value even with change in percentage load demand	80

List of Tables

2.1	Relationship between duty cycle and DC/DC converter voltages	20
2.2	Valid switch states for a 3-phase voltage source inverter	27
3.1	PV cell and module specifications	42
3.2	Terminal conditions of IEEE 14-bus system with 100 MVA base [7].	49
3.3	Transmission line characteristics of IEEE 14-bus system [7].	50
3.4	Load characteristics of IEEE 14-bus system [7].	50

Chapter 1

Introduction

Many have called solar radiation the fuel of photovoltaics (PV), since its attributes form the basis for PV system designs, from the construction of the system array to electric reliability of PV stand-alone systems. The understanding of solar radiation can be dated back to 1839 through the study of photoelectric effect by Edmund Becquerel [8], before the first solar cell was made by Daryl Chapin, Calvin Fuller and Gerald Pearson in 1954 [9]. Today, which is almost 70 years after this discovery, the same solar cell design is responsible for over 226GW global installation of PV, where China leads with about 43.5GW cumulative capacity [10].

Batteries in PV systems are arguably the most vulnerable component of the entire system. Design and operation faults such as array under sizing and charge controller breakdown can lead to battery failure making the system unable to deliver the anticipated power. The capacity of a battery is not fixed but instead depends on the

temperature, discharge current, state of life and other factors, which makes the complex electrochemical devices depend on a large number of material properties meeting a defined standard to function correctly. These batteries are mainly used to perform three main functions in PV systems: (1) as a buffer store to eliminate the mismatch between the power available from the PV array and the power demand from the load, (2) as an energy reserve device and (3) to prevent large and possibly damaging voltage fluctuations [11]

The power electronics converters provide a technology interface that enables efficient and flexible interconnection of different players such as renewables, energy storage devices, flexible transmission and controllable loads to the electric power grid [12]. Grid converters, sometimes called “synchronous converters” when compared to the synchronous generator in centralized power systems has a crucial role to play in future power systems based on smart grid technologies, since the distributed generation system will create more voltage levels needed to be managed.

1.1 Research Background

PV cell efficiency has been the focus of a significant amount of research in recent years with the emergence of more materials and technology for higher efficiency. Some research have focused on the type of materials recommended for PV cell designs [13], some authors have suggested that multi-junction solar cells will define our future cell

manufacturing process because of their promising high efficiency over the traditional crystalline silicon cells [14–18]. For large PV array plants, partial or uneven shading will lead to large row current difference. Researchers have proposed methods of minimizing PV row current by altering electrical properties of the PV array rather than the physical PV characteristics to achieve maximum power during partial shading [19–22].

Photovoltaic systems have been incorporated with different energy storage devices to increase the overall system performance where battery storage systems seems to be paramount. Some research works focus on the battery sizing [23–26] while others studied the types of converter suitable for different battery applications [27–30].

With the discovery of semi-conductor devices such as silicon carbide (SiC), capable of switching at high frequency, operating at high temperatures and capable of blocking high voltage researcher are focusing on new topologies and control strategies for PV system power electronics converters [31]. Research has also proposed a method of connecting multiple SiC IGBT-MOSFET devices in series to increase their voltage blocking potential and methods of suppressing the ground leakage current for PV inverter applications [32, 33]. A tri-port topology to interface with PV, battery, and three-phase grid with soft switching transformer is proposed in [34]

1.2 Thesis Outline

Chapter 1 introduces the research background for PV systems and the parameters to be considered for design. To refine the main goals of this research, literature reviews of solar PVs and control methods are also covered in this chapter.

Chapter 2 focuses on the theoretical fundamentals and gives an overview of the latest technologies and developments in PV systems, from the material models used for PV cell designs, to the control methods for the power electronics converters used by PV systems with battery support.

Chapter 3 discusses the configuration and associated control strategies of a multi-MW grid connected PV system. In which, grid integration is established by connection with a standard IEEE 14 bus test system in order to observe its steady state and transient effect with changes in electrical and environment parameters.

Chapter 4 presents an approach for expanding the capacity of an existing irrigation farm with additional pumps powered by PV. A novel control method for pumping system modulation is also introduced.

Chapter 5 concludes the thesis with a summary of work and original contributions. Suggestions for future work that can be extended based on the current research are also discussed.

Chapter 2

Conceptual Developments

2.1 Introduction

In early 2017, solar energy was described as the fastest growing source of renewable energy [35]. While other renewable sources of energy require large-scale implementations for maximum benefits and are typically recommended for power plant utility-level applications only, PV may be suitable for residential, commercial, industrial and power utility level deployments.

Power electronic converters are used to interface PVs and the power grid, since the legacy power grid is an AC system, while the PV output is DC. The characteristics of a PV system vary with environmental conditions such as irradiance and temperature. Power electronic devices can be used to ensure that PV systems are regulated for maximum output with changes in both environmental and electrical parameters.

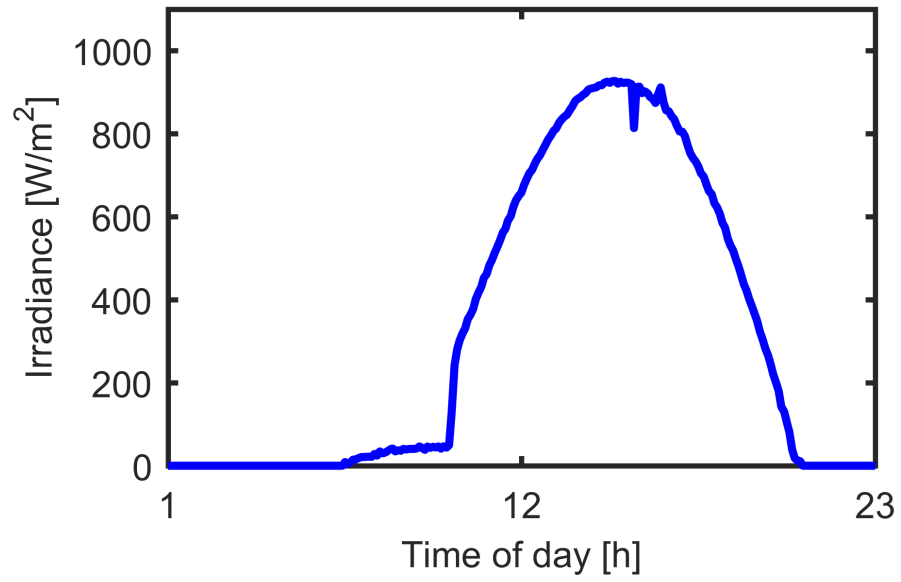
Photovoltaic systems can exist as stand alone system without grid connection or grid connected without energy storage. However, power swings are likely to occur

due to variation in array irradiance. In order to ensure that the PV is capable of producing constant power even during shading, energy storage devices in the form of batteries may be integrated into the PV system.

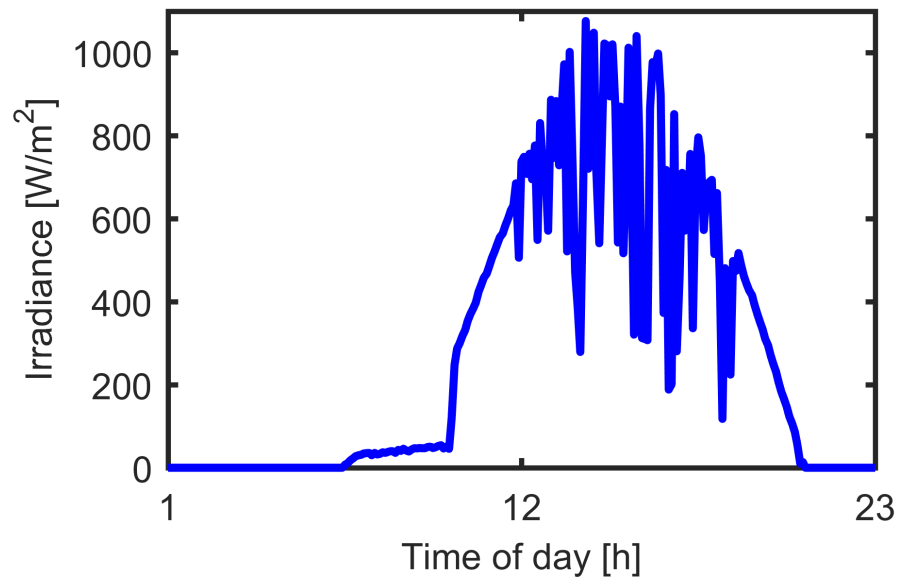
This chapter introduces the PV cells and array including the output characteristics of the cells and the need for maximum power point tracking(MPPT). Power electronic devices and controls needed for both DC-DC and DC-AC conversion are also discussed.

2.2 Photovoltaic Cells and Arrays

A PV cell is a specially designed PN junction or Schottky barrier device used for converting photons usually from sunlight directly into electricity. A typical photovoltaic cell is only capable of producing about 3 watts of electrical energy at approximately 0.5 DC voltage [36]. The efficiency of this cells depends on the technology used for the its fabrication. Noncrystalline, multi-crystalline and thin film technologies are the three dominating cell technologies with the noncrystalline cells having the highest efficiency and being the most expensive. There is a substantial amount of ongoing research to improve the arguably poor efficiency of PV cells. In June 2016, the U.S. Department of Energy’s National Renewable Energy Laboratory (NREL) validated the SunPower[®] X-Series silicon based solar panel to have reached an efficiency of 24.1% which was the highest at that time.



(a)



(b)

Figure 2.1: Irradiance variation for a full day, with example data sampled every 5min collected from the roof of RGAN building at University of Kentucky on a (a) clear and, (b) cloudy day [1].

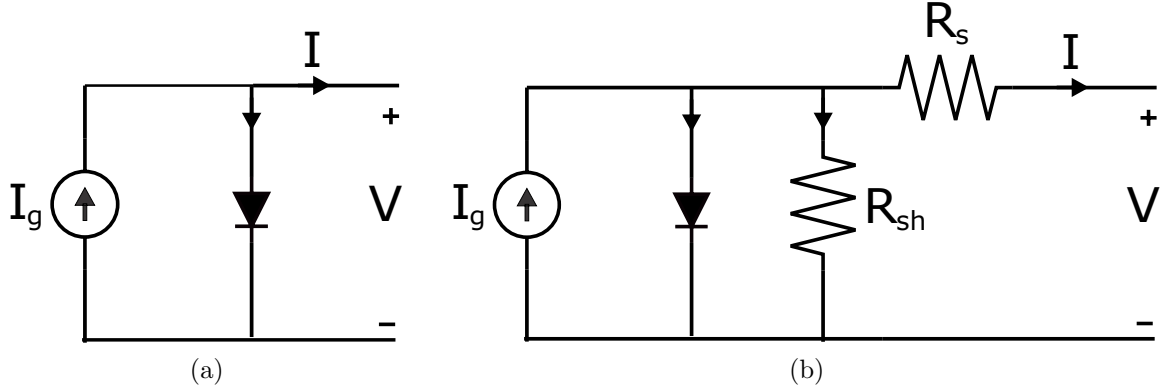


Figure 2.2: Equivalent circuit diagram of PV cell (a) ideal and, (b) real.

A PV cell is made of two slices of semi-conductor materials, usually silicon sandwich together to form a PN junction that absorbs photons mainly from sunlight, and allows incident photons to produce electron-hole pair with the atoms of the cell. The electric field at the PN junction then causes the photon-generated-electron-hole pairs to separate with the holes being attracted to the p-region and electrons drifting towards the n-region.

In order to study the electronic behavior of a PV cell, it is important to have an electrical equivalent model circuit made up of basic electrical components. A PV cell can ideally be represented as a current source connected in parallel to a diode, while a practical model includes a series and shunt resistance connected to the source (Fig. 2.2).

2.2.1 PV cell output characteristics

The amount of current and voltage available from a PV cell mainly depends on the amount of irradiance (illumination) on the surface of the cell and the ambient temperature. An increase in the level of irradiance leads to increase in the output current of the PV while higher temperature leads to a decrease in the output voltage. Equation (2.1) and (2.2) formalize the relationship between the PV cell current and voltage for an ideal and practical PV respectively.

$$I = I_g - I_o [e^{\left(\frac{qV}{KT}\right)} - 1], \quad (2.1)$$

$$I = I_g - I_o [e^{\left(\frac{V + IR_{sr}}{nKT_c/q}\right)} - 1] - \left(\frac{V + IR_{sr}}{R_{sh}} \right), \quad (2.2)$$

where, I_g represents the component of cell current due to photons; I_o , the saturation current; K , the Boltzmann constant ($K = 1.38 \times 10^{-23} \text{ J/K}$); q , the electron charge ($q = 1.6 \times 10^{-19} \text{ C}$); V , the output voltage; T_c , the cell temperature; R_{sh} , the shunt resistance and R_{sr} , the series resistance.

In (2.2), the photo-current I_g depends on the amount of solar irradiance falling on the PV cell and cell temperature. The photo-current relationship with solar irradiance (G) and cell temperature (T_c) can be given as:

$$I_g = I_{scR} \frac{G}{G_R} [1 + \alpha_T (T_c - T_{cR})], \quad (2.3)$$

where, I_{scR} is the short circuit current at the reference solar radiation G_R and the reference cell temperature T_{cR} . α_T represents the temperature coefficient of the photocurrent which is usually 0.0017A/K for silicon solar cells. At standard test conditions (STC) the reference irradiance is given as 1000W/m² at 25°C temperature. Another standard test condition is the photovoltaic for utility scale application test condition (PTC) where the reference irradiance is given as 1000W/m² at 20°C temperature.

The saturation current, I_o in equation 2.2 also known as the “dark-current” is a function of the cell temperature and the relationship is given by:

$$I_o = I_{oR} \left(\frac{T_c^3}{T_{cR}^3} \right) \exp \left[\left(\frac{1}{T_{cR}} - \frac{1}{T_c} \right) \frac{q e_g}{nk} \right], \quad (2.4)$$

where, I_{oR} is the saturation current at the reference temperature, e_g is the band gap energy of the solar cell material and n is the diode ideal factor which is typically 1.3 for silicon solar cells.

A simple PV circuit is designed in PSCAD/EMTDC environment and its parameters are described in Fig. 2.3. The PV module, which consists of a single PV cell is observed under different atmospheric conditions and operating load. An ideal variable DC source is connected to the PV through a diode, D in order to vary the output voltage of the PV cell, and the PV module input G (irradiance) and T (temperature) are independently varied. The output characteristics of the PV are largely dependent on the level of the irradiance and temperature as illustrated in Fig. 2.4. It can

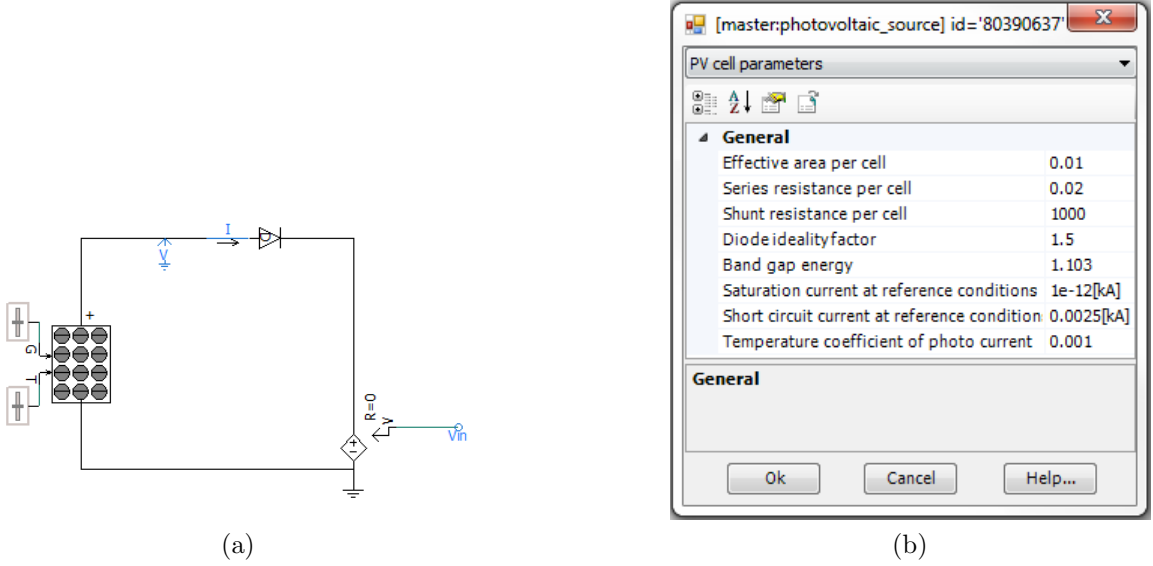


Figure 2.3: (a) Setup in PSCAD environment for a simple PV circuit with variable output voltage, and (b) PV cell properties dialog box in PSCAD.

therefore be observed that increase in level of irradiance leads to increase in current and a slight increase in output voltage, while increase in the cell temperature leads to a reduction in the output voltage of the PV. It can be concluded that a PV cells generates the highest amount of power at the coldest location with the highest level of solar irradiance.

Due to the low efficiency of the PV cell being typically about 20%, only a small percentage of the incident light energy is absorbed and converted to electricity leaving the remaining to be converted to heat, which leads to increase in the PV cell temperature. The PV cell temperature is a function of amount of solar irradiance G , the ambient temperature T_A and the nominal operating cell temperature (NOCT), which is the temperature the PV cell will reach without any load connected to it

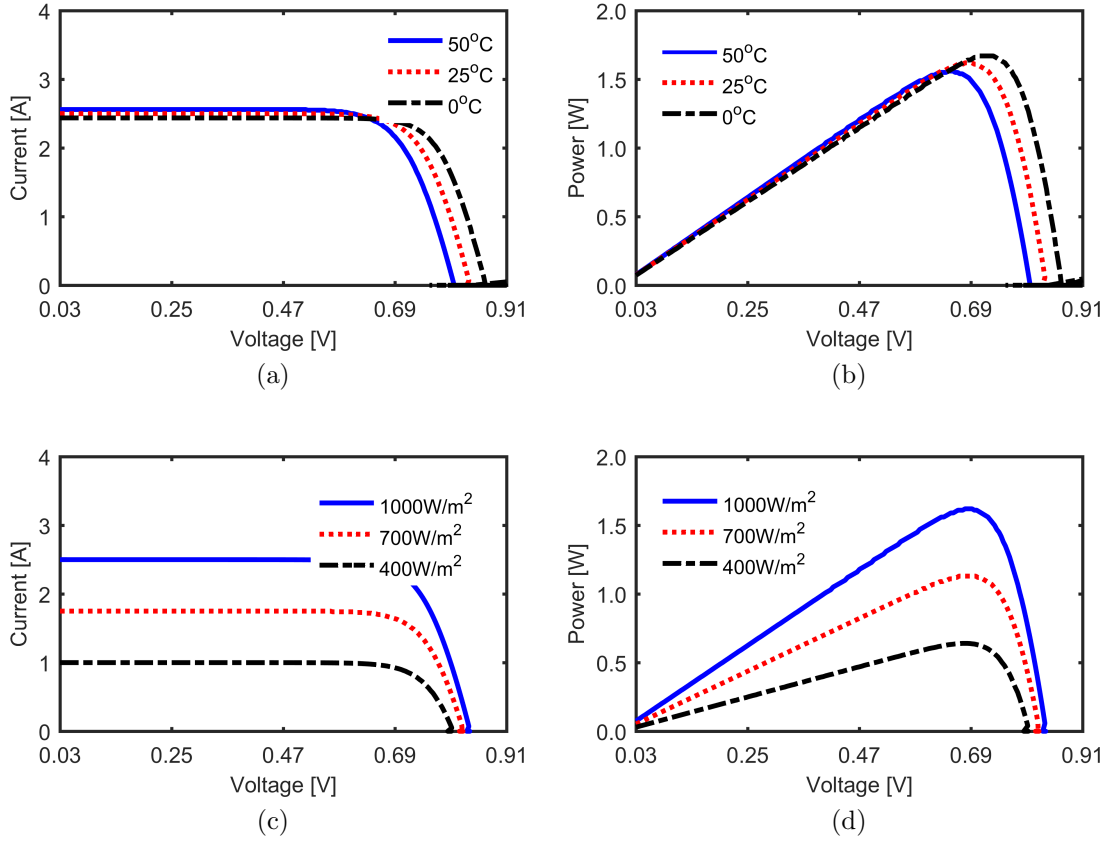


Figure 2.4: The cell output voltage and maximum power increases with decrease in cell temperature at constant $1000\text{W}/\text{m}^2$ solar irradiance (a) I-V curve, (b) P-V curve. Cell output voltage increases with increase in solar irradiance at constant 25°C cell temperature (c) I-V curve, (d) P-V curve.

(open-circuit), with air mass (AM) of 1.5 at 20°C, $G = 800\text{W/m}^2$ and wind speed less than 1m/s . The PV cell temperature, T_C ($^{\circ}\text{C}$) can therefore be calculated as:

$$T_C = T_A + \left(\frac{NOCT - 20}{0.8} \right) G. \quad (2.5)$$

2.2.2 PV module and array setup

A PV cell which is a fragile electrical component and typically about 156mm x 156mm in dimension [37] can be connected in series and parallel to form a PV module for voltage and power requirements. Common PV modules are made up of 54 to 72 cells and sometimes, more cells are needed to meet certain terminal requirements. Photovoltaic cells within a module may be shaded due to an external object or partial cloud cover, when PV cells within a PV module are shaded:

(a) The shaded cells may become reverse-biased and consume power instead of producing it, which therefore lead to loss in the total power output

(b) Potential failure of the entire PV module is possible when the heat generated as a result of individual shaded cell causes thermal stress on the surrounding cells which creates hot spots and local defects in the module

(c) Extreme shading within the PV module can generate reverse bias voltage that exceeds the solar cell breakdown voltage causing complete damage of the cell. Therefore, PV cells are connected in parallel to bypass diodes, which provide an

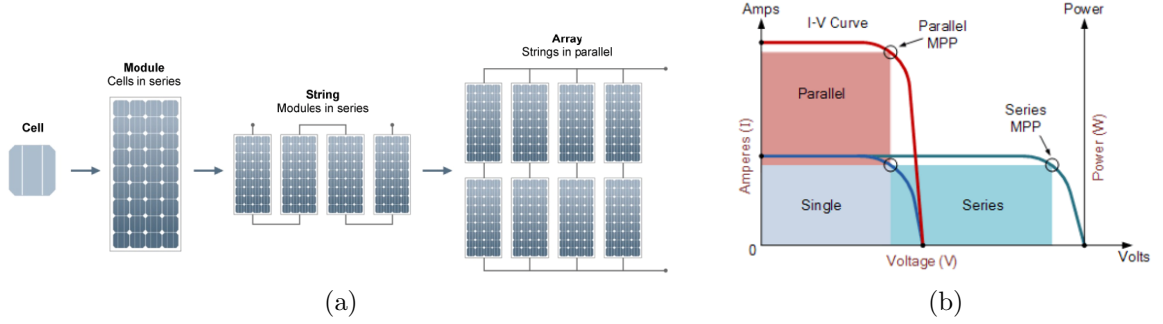


Figure 2.5: (a) Solar PV cell configuration from solar cell to solar array [2], (b) IV curve of solar PVs with different configurations [3].

alternate path for the current trapped in the cells. During random shading across the cells in a PV module, the output power reduction can be up to 91.9% without bypass diode installation [38]. A PV module could have each cell installed with a bypass diode, which could be non-overlapping or overlapping across cells.

A PV module consists of multiple cells connected in series and parallel, a string consists of modules connected in series while an array consists of modules connected in series and parallel as illustrated in Fig. 2.5a. When PV modules are connected in series, their individual voltages add up and the individual current of the PV modules sum up when they are connected in series as illustrated in Fig. 2.5b.

The photovoltaic PV array is a stationary object mounted at a particular location to absorb sunlight and convert it to electricity. Maximum amount of irradiance is received when the solar panel is perpendicular to the sun. However, the sun is not stationary, it is constantly changing its relative position to earth from morning to night and season to season making it impossible to have an orientation where the

solar panel will always receive maximum irradiance. The position of the sun in the sky is represented by the solar altitude and solar azimuth, solar altitude refers to the angle of the sun relative to the earth's horizon while the azimuth is the angle along the horizon, where the north corresponds to zero degrees, and increasing in a clockwise fashion. The solar azimuth and altitude at a particular location changes with respect to the time of the day and the day of the year. Solar constant is the average rate of radiant energy received from the sun on earth and varies with the day of the year. The solar constant for a particular day can be calculated using (2.6) where I_{solar} represents the solar constant and n represents the day of the year with January first being 1.

$$I_{solar} = I_o \left[1 + 0.034 \left(\frac{360n}{365.25} \right) \right]. \quad (2.6)$$

Solar panels will receive the maximum level of insolation when oriented at a tilt angle that corresponds to the latitude of the location, the azimuth however depends on the location of the panel with respect to the equator. PV panels located in the northern hemisphere receive maximum insolation when facing south (180°) while southern hemisphere is better oriented facing north. The maximum amount of sunlight is absorbed when solar panels are perpendicular to the sun which will only happen once a day if the PV panels are stationary. Solar trackers are devices used to automatically

trail the movement of the sun in the sky with either single-axis or dual-axis movement to ensure that the maximum amount of irradiance is received by the array at all times.

2.2.3 Maximum power point tracking

The maximum available power from a PV array depends on its electrical properties and atmospheric conditions at the point of installation while the operating point depends on the load connected to it. PV panels produce the maximum power when operated at the knee of the I-V curve as illustrated in Fig. 2.4. The technique for operating PV panels at the knee of the IV curve irrespective of the load connected to it is called maximum power point tracking (MPPT), which can be performed on individual PV panels instead of the entire array in the form of distributed maximum power point tracking (DMPPT). Typically, power electronic devices are used to vary the magnitude of the impedance seen by the PV array such that the output voltage of the PV array corresponds to the maximum power point (MPP) voltage of the PV array calculated by the MPPT algorithm. Perturb & observe and incremental conductance methods are the most commonly used algorithms for calculating the maximum power point of a PV array.

Perturb & observe is a widely used techniques for MPPT due to its simplicity and straightforward implementation process. This algorithm works by adjusting (i.e.

perturb) the output voltage of the PV array and observing the corresponding output power. When the output voltage of the PV is perturbed in a particular direction, an increase in output power signifies that the operating point is moving towards the MPP and the voltage is further perturbed in that direction. However, if perturbing the voltage in a particular direction leads to a decrease in the PV output power, the point of operation is moving away from the MPP, the algorithm therefore, perturbs the voltage in the reverse direction. This perturbation and observation continues and the system never reaches a steady state but instead oscillates around the MPP. The perturb and observe method has been modified by some authors to be able to quickly determine the correct MPP of the PV in rapidly changing atmospheric conditions. For example a modification where the irradiance changing factor is considered in every perturbation in order to determine the power change due to atmospheric conditions is proposed in [39].

Incremental conductance(InC) method requires more computation in the controller and keeps better track of changing conditions more rapidly compared to perturb and observe algorithm [40]. With incremental conductance technique, the MPP tracker can stop perturbing the output voltage of the PV when the MPP is reached. The MPP is determined by locating the point where $dV/dI = -I/V$. At the knee of the IV curve dP/dV is zero, dP/dV is negative when the MPPT is to the right of the MPP and positive when it is to the left of the MPP. The basic equations for this

technique are as follows [41]:

$$\frac{dI}{dV} = -\frac{I}{V}, \quad \text{at MPP,} \quad (2.7)$$

$$\frac{dI}{dV} > -\frac{I}{V}, \quad \text{left of MPP,} \quad (2.8)$$

$$\frac{dI}{dV} < -\frac{I}{V}, \quad \text{right of MPP.} \quad (2.9)$$

2.3 Power Electronics Converters and Electric Machines

Power electronic converters are electronic circuits used for controlling the flow of electrical energy. This typically involves the use of solid state electronics to control and convert electrical power from one form to another to achieve the specified requirements. Diodes, thyristors and transistors are examples of semi-conductors switching devices used in power electronic converters. Power electronic converters can be used to connect electrical sources to loads whose electrical requirement is different from the source output. In some cases, the power electronics are used for power transformation between AC and DC. These converters are also used for efficient control of electric machines and provide high reliability due to lack of moving parts.

Electric machines are electromechanical energy converters used to transforming electrical energy to mechanical energy and vice versa. Electric motors convert electrical energy to mechanical energy while generators are used to convert mechanical energy to electrical energy mainly through electromagnetic induction.

2.3.1 DC/DC converters

DC/DC converters are linear and switching converters used for transforming DC source voltage from one level to another. Linear converters maintain continuous current flow from input to the load while switching converters regulates same current flow by chopping the input voltage and controlling the average current flow through varying the duty cycle of the system. Another classification of DC/DC converters is the hard-switching pulse width modulated (PWM) converter which is more dominant as compared to the resonant and soft switching converters since it has high efficiency, constant frequency operations, relatively simple control, commercial availability of integrated controllers as well as ability to achieve high conversion ratios for both step-down and step-up application [42]. The four basic DC/DC topologies are buck, boost, buck-boost and Ćuk converters. A simple implementation of the converter topologies to show the variation of their output voltages with changes in their duty cycle was carried out in PSCAD environment (Fig. 2.6 and 2.7).

Table 2.1: Relationship between duty cycle and DC/DC converter voltages

Converter Topology	Output voltage
Buck converter	DV_{in}
Boost converter	$V_{in}/(1-D)$
Buck-boost converter	$-DV_{in}/(1-D)$
Cuk converter	$-DV_{in}/(1-D)$

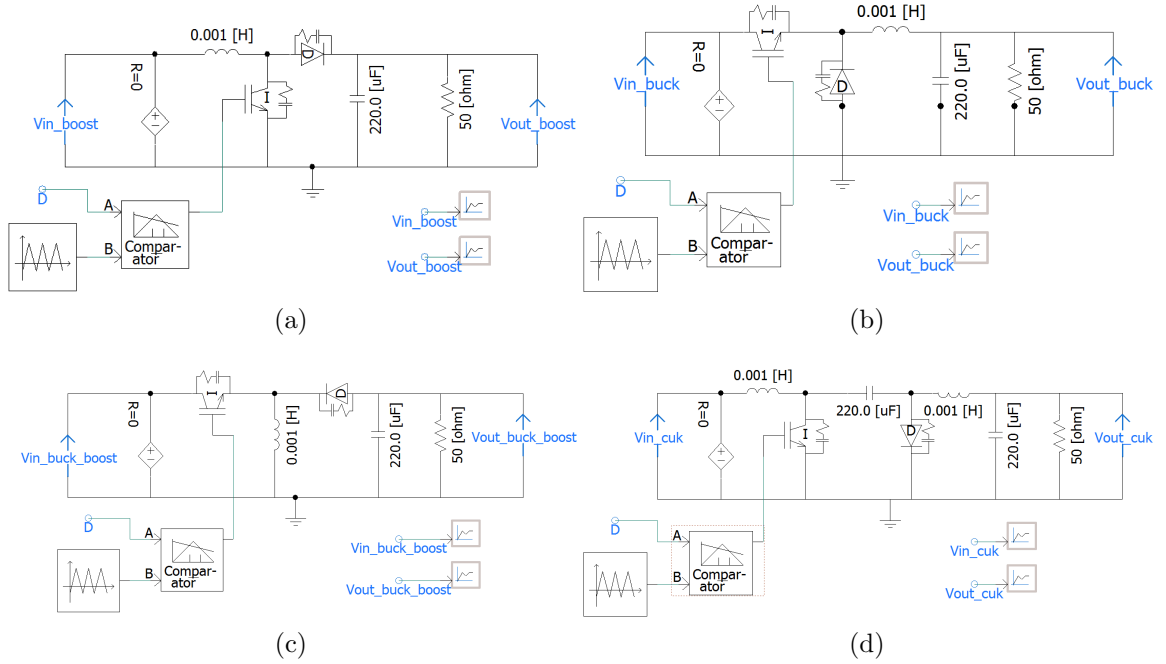


Figure 2.6: Schematic diagram in PSCAD/EMTDC for DC/DC converter (a) buck, (b) boost , (c) buck-boost and (d) Cuk

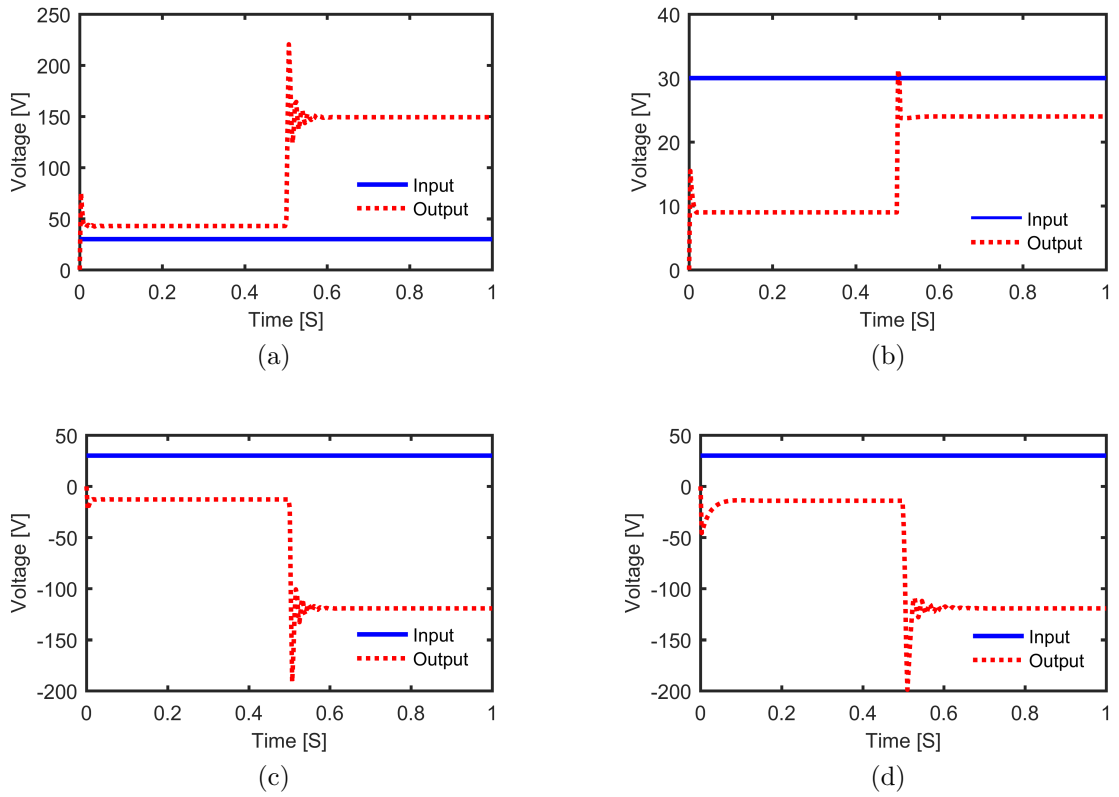


Figure 2.7: Input and output voltage result in PSCAD/EMTDC with duty cycle changing from 0.3 to 0.8 at 0.5secs simulation time for DC/DC converter (a) boost, (b) buck , (c) buck-boost and (d) Ćuk

2.3.2 AC/DC converters

A rectifier or AC-DC converter is an electrical device made up of power electronics devices used to convert AC to DC , while DC-AC converters also known as inverters convert DC to AC. AC-DC converters are primarily used in power supply systems to provide DC power to electronic equipments, computers, battery charge controllers, DC and inverter fed drives etc. Rectifiers can be grouped into uncontrolled rectifiers whose output solely depends on the input power and controlled rectifiers whose output waveform also depends on an external control system. Uncontrolled rectifiers are typically made of diode and can be categorized into full bridge and half bridge diode rectifiers for both single phase and three phase systems.

Diode bridge rectifiers with output capacitive filter draw non-sinusoidal currents, which cause low input power factor [43]. Half wave rectifiers which only produce an output for half electrical cycle has an advantage of using less power electronic devices as compared to the full bridge rectifier. A single phase full wave rectifier can also be implemented using 2 diodes if a transformer with center tap secondary side is included in the configuration, without a center tap transformer, the system will require 4 diodes as shown in figure 2.8. Full wave rectifiers have better performance when compared to half wave rectifiers, which have high ripple factor, low rectification efficiency, low transformer utilization factor and leading to saturation of the transformer secondary windings. For the described circuit diodes D1 and D2 conduct for the positive half

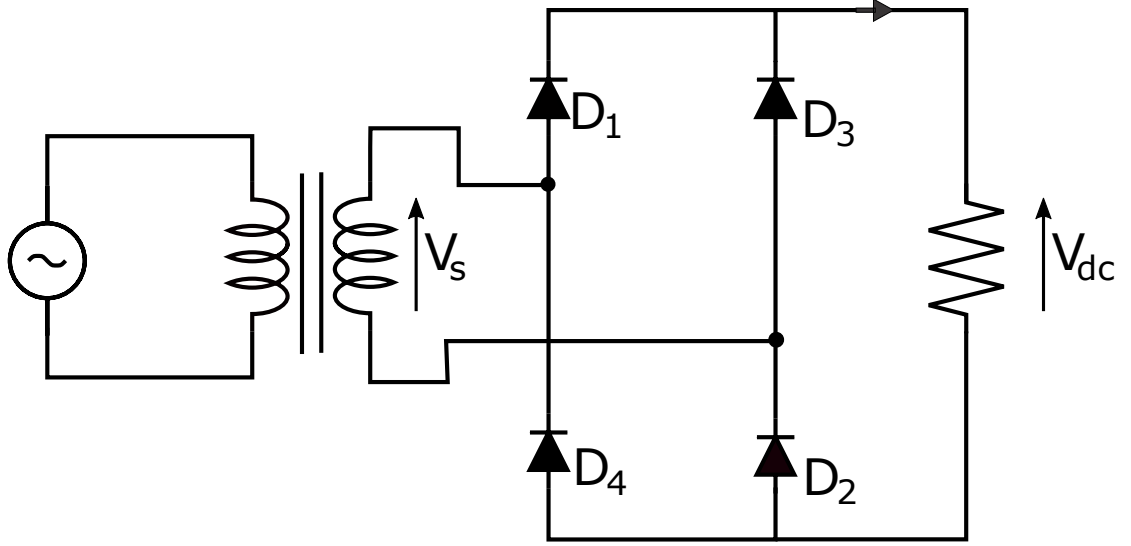


Figure 2.8: Circuit diagram for a full bridge uncontrolled diode rectifier.

cycle and diodes D3 and D4 conducts for the negative half cycle. The supply voltage V_s is given as $V_m \sin \omega t$, the average load voltage V_l is represented as V_{dc} . The relationship between the AC voltage and the DC voltage of both full-wave rectifier and half wave rectifier is given as:

$$V_{dc} = \frac{1}{2\pi} \int_0^\pi V_m \sin \omega t d(\omega t) = \frac{V_m}{\pi} = 0.318V_m \quad \text{for half bridge,} \quad (2.10)$$

$$V_{dc} = \frac{1}{\pi} \int_0^\pi V_m \sin \omega t d(\omega t) = \frac{2V_m}{\pi} = 0.636V_m, \quad \text{for full bridge.} \quad (2.11)$$

The rectification ratio, which is a measure of the effectiveness of rectification for a half bridge rectifier is only 40.5% while that of a full bridge rectifier is 81% [42].

Replacing the diodes in uncontrolled diode bridge rectifiers with a thyristor (or transistor) makes it a controllable rectifier. Controlled rectifiers are AC to DC power converters used to convert fixed frequency and voltage AC supply into variable DC power output. Thyristors use phase control to obtain variable DC voltage by controlling the phase angle (trigger angle) at which the thyristors are triggered. The controlled rectifier setup can be divided into three parts: the power circuit, control circuit and triggering circuit. The power circuit consists of the voltage source, load and power electronics devices. The control circuit is a logical circuit that controls the way the switches are being operated and the triggering circuit consists of buffers, pulse transformer opt coupler used for converting the digital responses of the control circuit to analog signal used to driving the power circuit.

Just like the diode bridge rectifier, the full bridge rectifier also has two thyristors allowing flow of AC power for the positive half, and the remaining two allowing the flow of electricity for the negative half cycle. Unlike diodes, which automatically conducts when forward biased, Thyristors need a suitable gate trigger pulse to turn on. If the supply AC voltage is given as $V_m \sin \omega t$ where input voltage is positive from $0 < \omega t < \pi$ and negative for $\pi < \omega t < 2\pi$, if the rectifier is triggered at $\omega t = \alpha$ the α is called the *firing angle* of the rectifier. Equation 2.12 describes the relationship between the AC supply voltage and the average load voltage for a single phase bridge controlled rectifier. The average load voltage of the system can therefore be varied

by regulating the firing angle of the thyristor, which can be applied in DC motor controls as well as uninterpretable power supply systems (UPS).

$$V_{dc} = \frac{1}{\pi} \int_{\alpha}^{\pi+\alpha} V_m \sin \omega t \, d(\omega t) = \frac{2V_m}{\pi} \cos \alpha, \quad (2.12)$$

DC to AC converters also known as inverter is a device that converts DC power from a particular source to corresponding AC power at a specified voltage, phase and frequency through the use of controlled semi-conductor devices. The output AC waveform of an inverter can either be voltage controlled or current controlled. Voltage controlled inverters also known as voltage-source inverter (VSI) are the most popular and widely used inverter, which independently controls the AC output voltage while current controlled inverters (current-source inverter) independently controls the AC output current. Inverters are further classified into offline and online inverters. Offline inverters are used when the inverter is the only source for the AC load, while online inverters are used when the inverter is part of the common power supply lines to the load and operated at same frequency and similar magnitude with the other sources connected to the load.

The standard topology for a 2-level voltage source inverter with switches which can be made of IGBT, transistors or any other power electronic device capable of meeting the electrical demand of the load is illustrated in Fig. 2.9. An example PWM technique is the sine-triangle PWM, wherein, a sinusoid of the desired frequency is

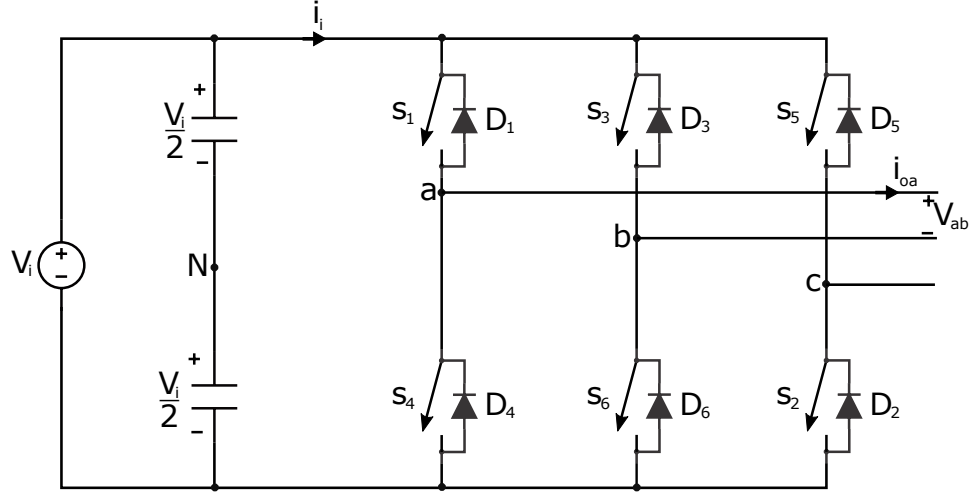


Figure 2.9: Circuit diagram for a 3-phase voltage source inverter

compared with a high frequency ramp and its output is used to drive the switches. Table 2.2 shows the valid states for the described 3-phase voltage source inverter. It is important to note that adjacent switches (S_1 and S_4 , S_3 and S_6 or S_5 and S_2) cannot be turned on at the same time since this will primarily lead to the short circuit of the DC link. The control for these switches are always inverted with a delay known as dead time so that the turn off time of one switch will be elapsed before the adjacent one will be turned on. States 7 and 8 in Table 2.2 have zero AC line voltages and are therefore ignored, AC voltage waveform is produce by the manipulation of the other 6 states. The output of the inverter is AC, at the frequency of the modulating signal, and its magnitude is proportional to the magnitude of the modulating signal.

Table 2.2: Valid switch states for a 3-phase voltage source inverter

State no	Switches ON	Switches OFF	V_{ab}	V_{bc}	V_{ca}
1	S_1, S_2 and S_6	S_4, S_5 and S_3	V_i	0	$-V_i$
2	S_2, S_3 and S_1	S_5, S_6 and S_4	0	V_i	$-V_i$
3	S_3, S_4 and S_2	S_6, S_1 and S_5	$-V_i$	V_i	0
4	S_4, S_5 and S_3	S_1, S_2 and S_6	$-V_i$	0	V_i
5	S_5, S_6 and S_4	S_2, S_3 and S_1	0	$-V_i$	V_i
6	S_6, S_1 and S_5	S_3, S_4 and S_2	V_i	$-V_i$	0
7	S_1, S_3 and S_5	S_4, S_6 and S_2	0	0	0
8	S_4, S_6 and S_2	S_1, S_3 and S_5	0	0	0

2.3.3 Electric machines for pump systems

A pump is a device used to compress, raise or transfer fluids from one point to another. Pumps are generally classified into centrifugal pumps and positive displacement pumps. In centrifugal pumps, Head and flow is produced by increasing the velocity of the fluid flowing through the machine with a rotating vane impeller allowing the fluid to be flung out, while the latter operates by allowing the fluid to flow into an open cavity before displacing a certain volume of the fluid leading to delivery of constant volume of liquid for each cycle against varying discharge pressure or head. Centrifugal pumps are the most common type of pumps, which can be mechanically rotated using an induction motor or a permanent magnet synchronous motor in AC applications. A non-linear parabolic relationship exists between the load torque and motor speed in motor driven pumps, which is given in (2.13), where T_L is the load

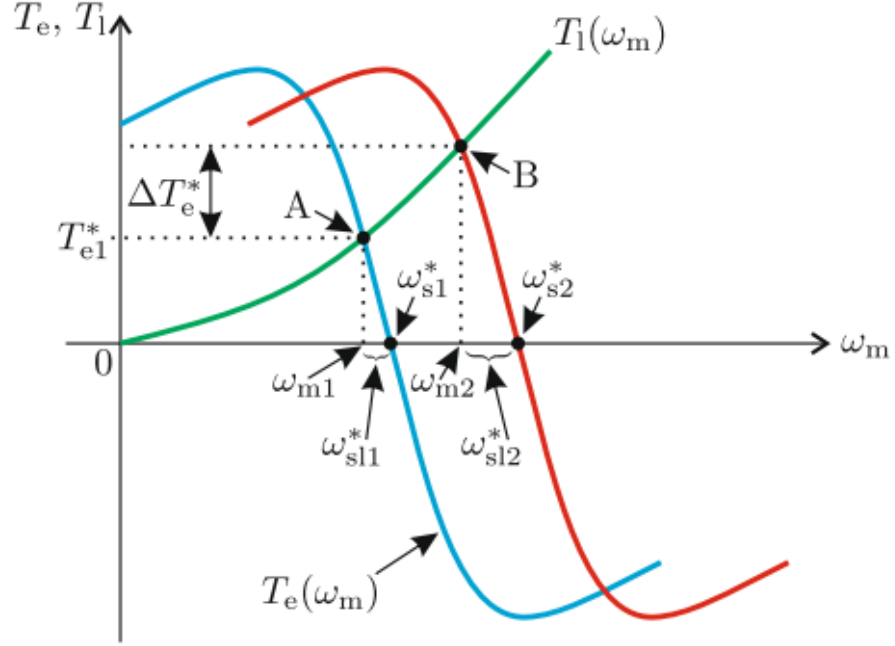


Figure 2.10: Steady state torque-speed curve for a typical induction motor (T_e) and a pump load (T_l). The operating point is at the intersection of the two curves (A or B) [4].

torque and ω is the load speed.

$$T_L \propto \omega^2, \quad (2.13)$$

Induction motor, also known as asynchronous motor is an electric motor, which allows AC to be supplied to the stator winding in a manner that produces rotating magnetic field. The rotating magnetic field in turns induces electric current in the rotor conductor. Interaction between the magnetic flux and induced currents exert a torque on the rotor that causes rotation. The steady state point of a motor driven

pump is found when the pump torque is equal to the torque produced by the machine as shown in the load torque/shaft-speed characteristic illustrated in Fig. 2.10. The speed of an induction motor can be varied by controlling the applied voltage, rotor resistance, stator frequency or in some cases, pole variation. In most application, the classic voltage to frequency control (V/f) is used since it entails a simple drive control. When the stator resistance of an induction motor is neglected the torque curve is reduced to the Kloss equation, which is given as;

$$T_{em} \approx \frac{2T_{max}}{\frac{s}{s_{max}} + \frac{s_{max}}{s}} \quad , \quad (2.14)$$

where T_{em} is the electromagnetic torque, T_{max} the breakdown torque, s is the slip and s_{max} is the slip at the breakdown torque. Figure 2.11 shows the block diagram of a simple V/f control. This control maintains the speed of the induction motor at a reference speed ω_s^* irrespective of the stator resistance by determining the voltage amplitude and phase angle required to drive the induction motor at the reference speed [4].

A permanent magnet synchronous motor (PMSM) is an AC electrical motor that has its field excitation provided by permanent magnet placed on the rotor and produces a sinusoidal back EMF waveform. Equation 2.15 describes the three-phase model of the permanent magnet synchronous motor where i_d and i_q represent the q and d axis currents, L_q and L_d represents d and q axis inductances, V_q and V_d

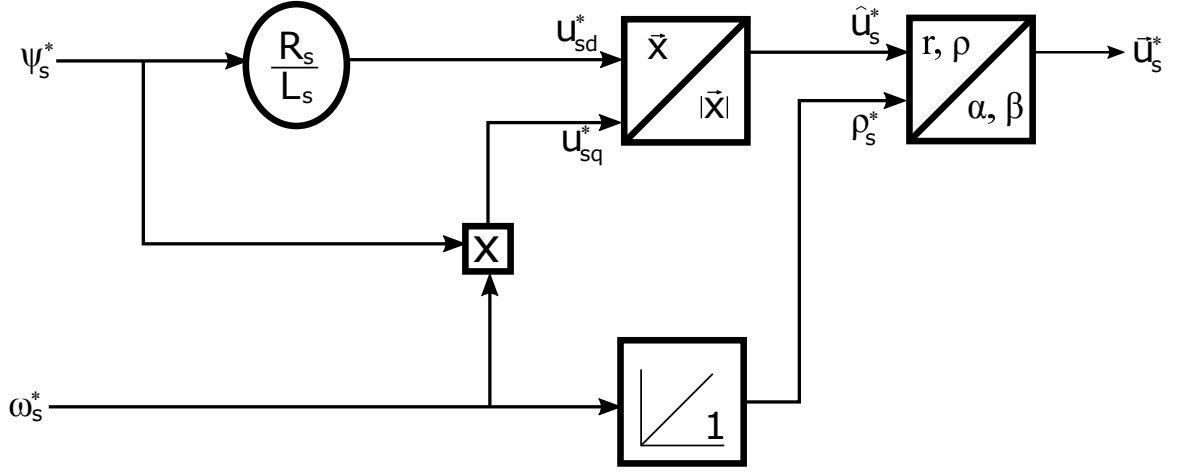


Figure 2.11: Block diagram of V/f control structure with stator frequency reference input

represents d and q axis voltages, λ induced flux amplitude, R the stator windings resistance, ω_m is the angular velocity of the rotor, and p is the number of pole pairs.

$$\frac{d}{dt}i_d = \frac{1}{L_d}v_d - \frac{R}{L_d}i_d + \frac{L_q}{L_d}p\omega_m i_q, \quad (2.15)$$

$$\frac{d}{dt}i_q = \frac{1}{L_q}v_q - \frac{R}{L_q}i_q - \frac{L_d}{L_q}p\omega_m i_d - \frac{\lambda p\omega_m}{L_q}, \quad (2.16)$$

$$T_e = \frac{3}{2}p[\lambda i_q + (L_d - L_q)i_d i_q]. \quad (2.17)$$

Permanent magnet synchronous machines are primarily used in building high efficiency and performance drive where a motor control with smooth rotation over the entire speed range is desired. Permanent magnet synchronous machines are capable of producing full torque control even at zero speed through the use of vector control

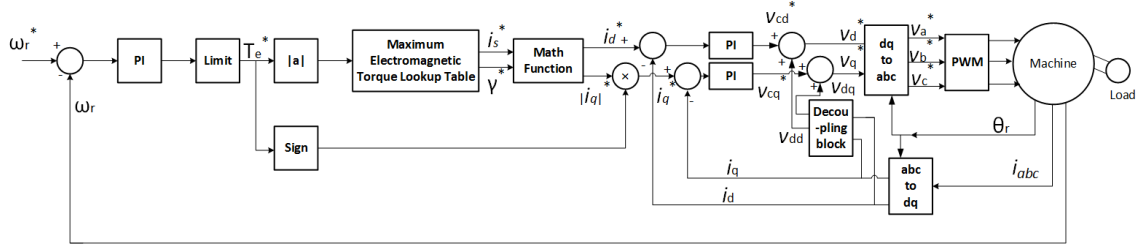


Figure 2.12: Block diagram of vector control for PMSM [5]

techniques also known as field oriented control (FOC), which also allows fast acceleration and deceleration of the motor. FOC algorithm decomposes the stator current of PMSM into magnetic field and torque generating component, which allows either of the component to be independently controlled. In order to perform vector control on a PMSM as shown in figure 2.12, the motor phase current are measured and transformed into the two phase (α, β) and (d, q) using Clarke and Park transformation, which requires the knowledge of the rotor position angle of the motor obtained either from an encoder or by sensor-less control techniques. This transformation produces the stator current torque (i_q) and the flux (i_d), which can be regulated for independent speed and torque control. The stator voltage corresponding to the controlled current in d-q domain is therefore transformed back to the abc domain before PWM technique is used to generate the gating signals for the inverter.

2.4 Battery Energy Storage Systems (BESS)

The world is trying to reduce its dependence on fossil fuels and concentrate more on generating power using renewable sources of energy. But renewable sources of energy such as wind and solar, which have the lowest carbon emissions and water usage have intermittent availability. For this reason, energy storage devices are essential component of future energy system that make use of large amounts of renewable energy. Energy storage system can be classified into mechanical, chemical, electrochemical, electrical and thermal. Among these storage devices, electrochemical energy storage devices in the form of batteries are the most widely used due to their ability to meet almost all types of power demand.

This BESS can be collocated with renewable energy resources to improve system stability through frequency response. They are also used as ramp control to improve the economics of renewable generators by leveling the output of solar generators [44]. In most BESS, the battery charges from the renewable energy source during excess energy generation or when energy from the grid is cheap and then uses it to support the renewable generator power output.

2.4.1 BESS management

Since BESS typically consists of more than one battery cell, its management system ensures efficient and safe operation of these batteries. This features control such

as effective cell balancing, cooling and ventilation, data acquisition, communications and interfaces between subsystems. Parameters such as terminal voltages, current and temperature of the batteries can be monitored and controlled in a *centralized* fashion where data is collected from individual cells and sent to the main management board for processing, *modular* topology, where data collected from each cell is processed by a slave control board before being sent to the main management board for process or *distributed* topology which allows each cell to have an electronic board and main controller responsible for communication, fundamental computations as well as calculating the state of charge (SOC), state of health (SOH) and state of life (SOL) are possible.

State of charge refers to the percentage charge available in a battery as a fraction of the nominal value (i.e capacity), which can be estimated based on the battery current, temperature and number of lifetime cycles. The performance of battery deteriorate after every cycle, and SOH is the remaining battery capacity for the current cycle as compared to the original battery capacity at first cycle. The time when the battery should be replaced is determined by the battery SOL, which also refers to the remaining useful life before its decommissioned.

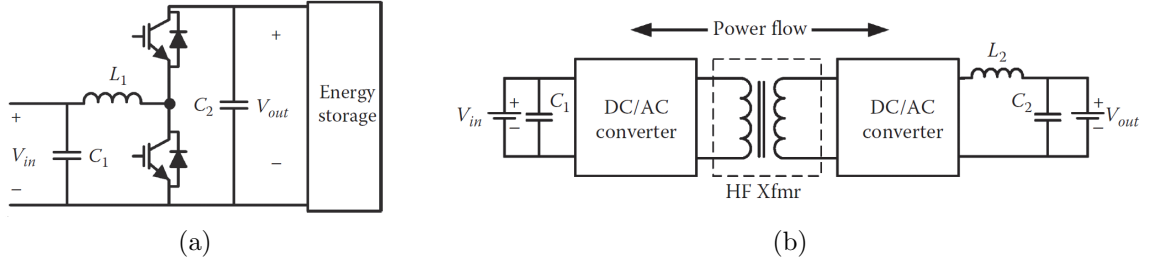


Figure 2.13: (a) Non- isolated half-bridge DC/DC converter, (b) voltage-fed isolated DC/DC converter [6].

2.4.2 BESS interface

Batteries are typically interfaced to the grid via power electronic converters. These converters exist as DC/AC converters, non isolated DC/DC converters and isolated DC/DC converters. The traditional six-switch H-bridge voltage source converter, which uses the most common PWM based closed-loop control technique to regulate DC link voltage regulation at close to unity power factor can be regarded as a bidirectional DC/AC boost-type converter.

Non-isolated DC/DC converters have simpler design, control and implementation due to the reduced amount of components, and they also provide a relatively high efficiency at lower cost. This system connects energy storage device to a DC bus and controls the flow of current by varying the voltage seen by it. Isolated DC/DC converters comprise of two high frequency inverter and rectifier connected back to back through a high frequency transformer which is used to provide galvanic isolation between the input and output sources (Fig. 2.13).

2.5 Summary

This chapter introduces the major devices and control strategies needed in a PV system. The PV cell output characteristics depends on the amount of irradiance present and the ambient temperature. The operating point can be determined by varying the equivalent impedance seen by the PV through the use of DC-DC converters controlled by MPPT algorithm. Energy storage devices such as batteries can be used to regulate the output power from renewable energy sources to ensure the continuous flow of high quality electricity. DC-AC converters are used to interface both the battery and PV array to the grid AC loads or other connected to it. For example, electrical machine.

Chapter 3

Integrating PV and Energy Storage Connected to the IEEE 14 Bus Modified Test System

This chapter discusses layout of a multi-megawatt grid connected solar PV farm integrated with battery energy storage system (BESS). The PV system is divided into several sections, and each section has its own DC-DC converter and a two-level inverter with grid oriented voltage control. The PV farm is connected to a modified IEEE-14 bus, on which different operation modes are demonstrated.

3.1 Introduction

The future smart grid is expected to be integrated with a substantial proportion of renewable energy. In 2016, the U.S department of energy reported that 24.42GW PV was installed from 2010-2015 and 56% of the installations were utility-scaled [45]. It is therefore important to study the effects of connecting multi-megawatt PV

systems to the existing power grid. A substantial amount of literature exists on PV systems connected to the grid, the focus of some of these literatures is on maximum power point tracking (MPPT) techniques. Incremental conductance (InC), perturb and observe method (P&O) and its derivatives are commonly used techniques for MPPT [46]. Some authors discuss the THD of the current injected to the grid, as well as other techniques such as short circuit current pulse method and fuzzy logic based controllers [47–49]

Other areas of research include DC-DC converter topologies, solar inverter topologies, and single stage power converter topologies [50–54]. Since irradiance inequality between panels connected in series may limit the power output, the focus of some of the work is on array reconfiguration to equalize irradiation [55]. Other papers propose module integrated converters, such that the maximum power point (MPP) of each module can be tracked, yielding maximum energy extraction [56]. Module integrated DC-DC converters connected to a central DC-AC converter is proposed in [57].

Each section of the system contains a PV array, transformer, DC-DC and DC-AC converters connected in parallel and interfaced to the grid as illustrated in Fig.3.1. With appropriate control the 2-level inverters may be cascaded in order to obtain a multilevel output voltage waveform. In this approach, each inverter is interfaced to the grid via a 2-winding transformer, which is not the only possible arrangement since a 3-winding transformer can also be used to interface the inverters in multiples of two

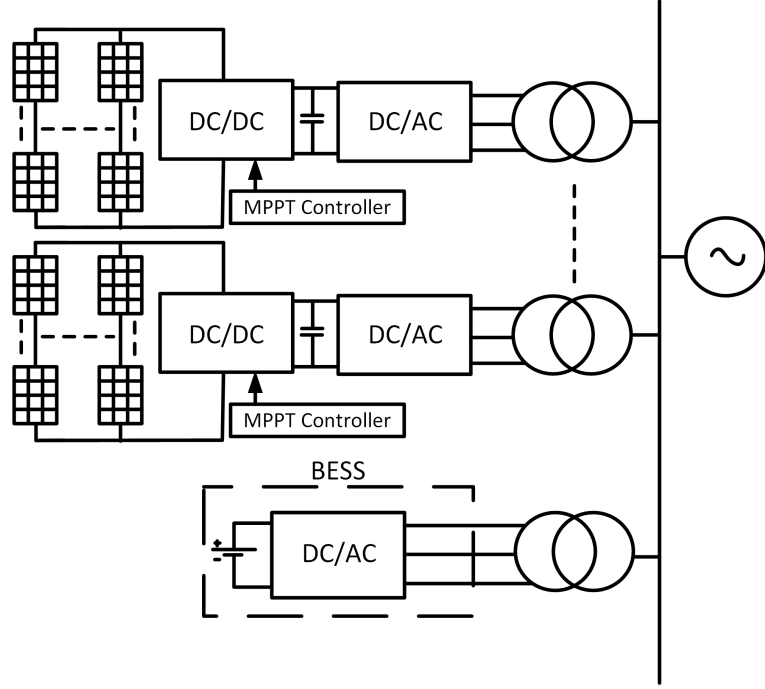


Figure 3.1: Schematic of a grid tied solar PV system consisting of several units in parallel with individual transformer connected to the grid for generality since design can also be implemented with a single transformer. The battery energy storage system is connected to the grid through its own inverter and transformer as well.

or all the inverters connected to one transformer. A battery energy storage system (BESS) is installed to supply power in case of partial or complete shading. When battery state of charge (SOC) is lower than its minimum during shading, adjacent synchronous generators supply the deficit power. This PV system with BESS is connected to the IEEE 14 bus and the entire system is modeled and simulated using PSCAD/EMTDC.

3.2 PV System

For high power applications, it is common to divide the PV plant into several sections (Fig. 3.1) to meet power conditioning electronics requirements [52, 58]. In each section, the PV array is connected to a buck converter used to maintain the PV array output voltage at its maximum power point(MPP). [57] recommends the use of buck converters for maximum power point tracking when multiple strings are connected within the PV array. The buck converter is connected to a two-level central inverter through a DC link capacitor , which is typically a two level inverter. The power circuit diagram of one unit modeled and simulated in PSCAD/EMTDC (Fig. 3.2).

3.2.1 PV array

A PV cell is an electrical device, which uses photovoltaic effect to convert light energy directly into electricity. PSCAD/EMTDC and [59] use the Norton equivalent circuit to represent its PV cells. The current and voltage relationship is given as:

$$I_{cell} = I_g - I_o \left[e^{\left(\frac{q(v + I_{cell}R_{sr})}{nKT_c} \right)} - 1 \right] - \left(\frac{v + I_{cell}R_{sr}}{R_{sh}} \right), \quad (3.1)$$

where, I_g , the photo current generated; I_o , the saturation current; K, the Boltzmann constant; q, the electron charge; V, the output voltage; T_c , the cell temperature; R_{sh} , the shunt resistance and R_{sr} , the series resistance.

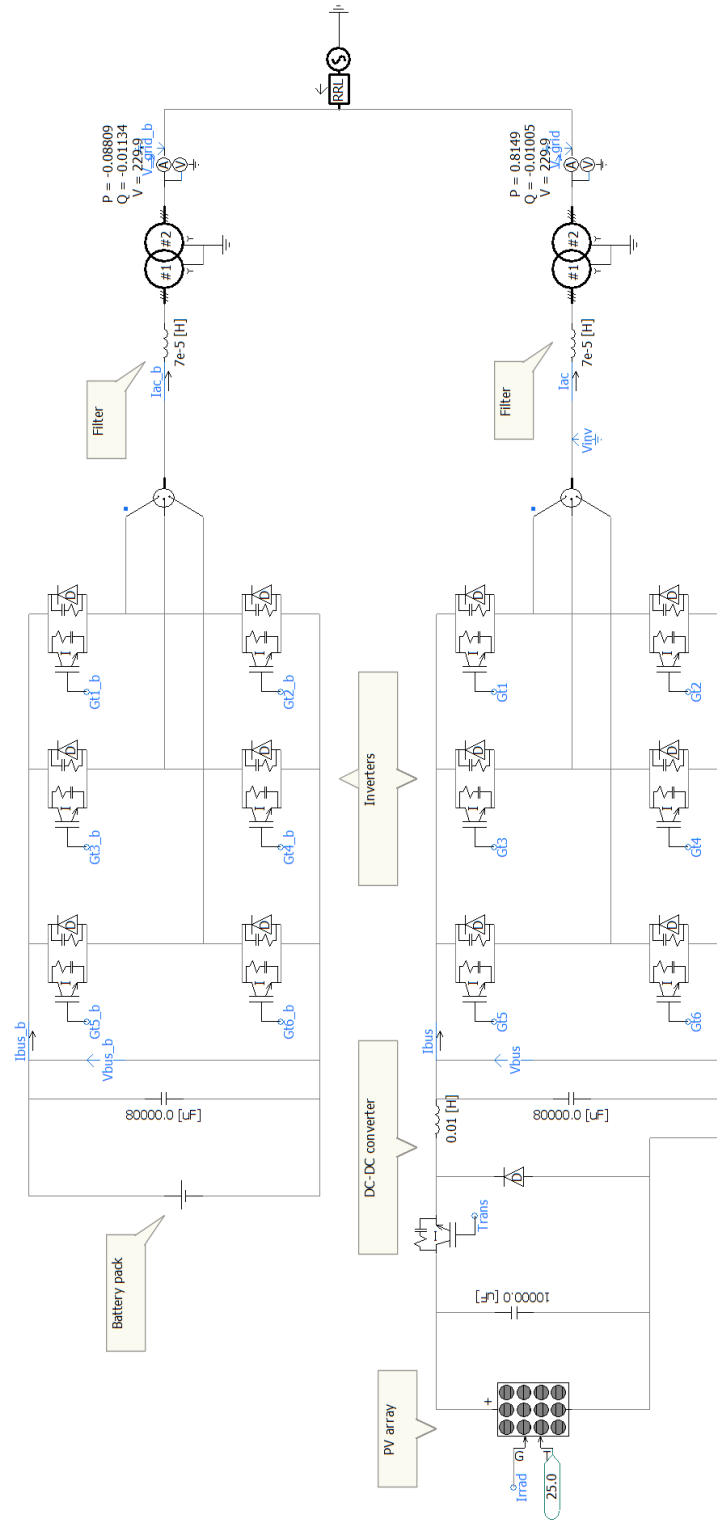


Figure 3.2: Power circuit diagram in PSCAD simulator showing the solar PV panel, DC-DC converter, 2-level inverter, transformer and grid. Practical implementations may use a Δ -Y transformer also.

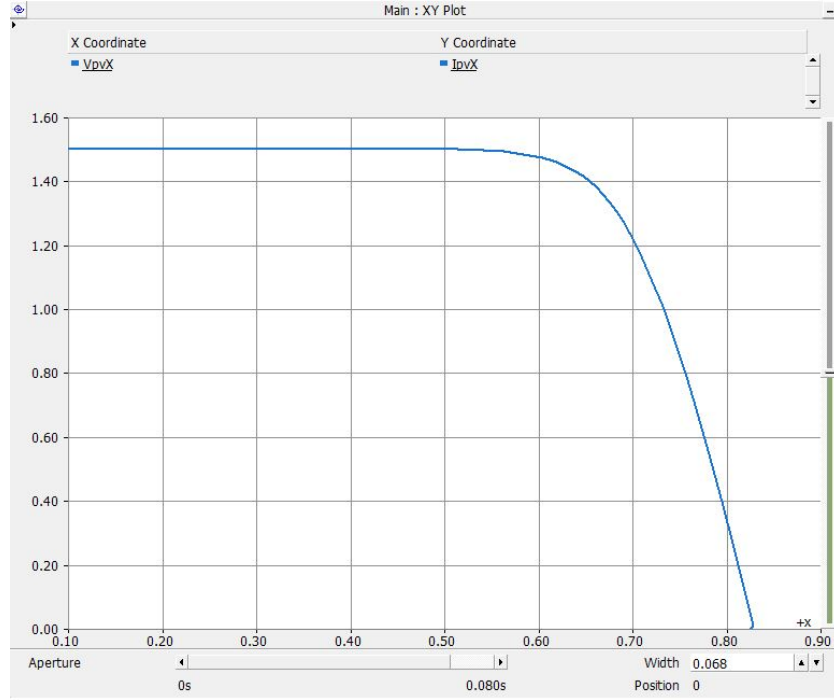


Figure 3.3: I-V characteristic of PV array at 25° and $1000\text{W}/\text{m}^2$ solar irradiance. For maximum output power, it is recommended to operate the PV at the knee of the curve.

Open circuit voltage of a PV module depends on the type of material used for the cell design and typically varies from 23.3 to 44.2V when tested under standard conditions [60]. The PV module in this system consist of 2 parallel strings with 40 PV cells in series per string to yield an open circuit voltage of 43.7V and short circuit current of 9.12A per module under standard test conditions (STC). The PV array used in this study consists of 160 strings of PV modules with 24 modules connected in series per string in order to restrict the DC bus voltage below 1kV. Figure 3.3 illustrates the current-voltage relationship of the PV array for a single unit at $1000\text{W}/\text{m}^2$ solar irradiance and 25° temperature.

Table 3.1: PV cell and module specifications

Parameters	Value
Cell open circuit voltage (V)	1.09
Cell short circuit current (A)	4.56
Module open circuit voltage (V)	43.7
Module short circuit current (A)	9.12
Maximum power (W)	260

3.2.2 MPPT

There exists a compound relationship between the operation of a PV cell and its environmental condition. At any operating environmental condition, there exists a point where the current and voltage values result in maximum output power, which is typically at the knee of the PV current-voltage curve. MPPT is used to ensure that PV provides the maximum output power at every atmospheric condition. In the studied model, the output voltage (V_{pv}) and current (I_{pv}) of the PV array is continuously measured and passed through a filter before being fed to the MPPT block, which uses incremental conductance method to determine the reference voltage (V_{mppt}) corresponding to the MPP as illustrated in Fig.3.4. A PI controller is employed in order to ensure V_{pv} is equal to V_{mppt} by varying the duty cycle of DC-DC converter, which is compared with a high frequency triangular signal generator for producing the IGBT gating pulses.

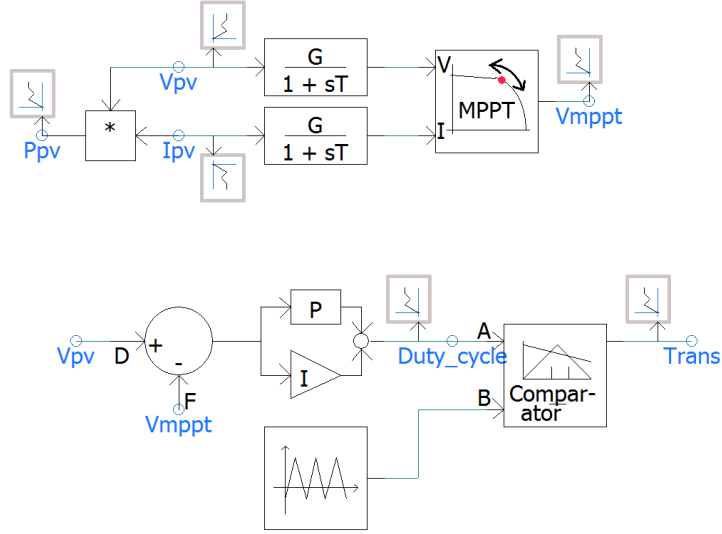


Figure 3.4: Control diagram for DC-DC converter using blocks from the PSCAD library.

3.3 Grid-Connected Inverter

The PV system is installed with a two-level inverter, which is a widely available technology that is relatively inexpensive and has been proven to be reliable for relatively small inverters below 1MW. The central 2-level inverter considered in this study has some limitations, including large filter size in order to meet the required THD standards and higher voltage rating for power electronic devices compared to the multi-level inverter. As mentioned previously, the PV plant consists of sections with their own DC-DC and DC-AC converters connected in parallel. The requirement of large filter size can be counteracted by the interconnection of inverter pairs in adjacent sections in cascade as shown in Fig. 3.5. Three - level output is obtained

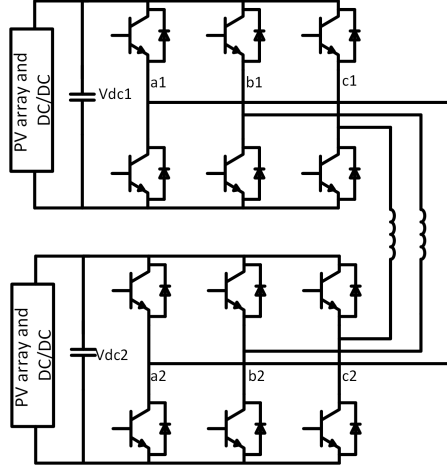


Figure 3.5: Schematic diagram of proposed 3-level inverter formed by cascading two 2-level PV inverters. More levels may be obtained by cascading more inverters in the system.

by maintaining the DC link voltages at the same value, and four level output can be obtained by maintaining $V_{dc2} = \frac{V_{dc1}}{2}$, while two level output is obtained when either one of the DC link voltages is zero [61]. The DC link voltages can be maintained at the desired value by absorbing the required active power from the grid. Alternatively, the inverters in three adjacent sections may be interconnected together to obtain a 4 level output, with the predominant harmonic frequency at 3 times the switching frequency [62].

The control block diagram of the voltage oriented control inverter used in each section is illustrated in Fig. 3.6. In this control, the phase locked loop (PPL) block generates ω from the instantaneous measurement of the grid voltages (V_{abc}), ω is used in reference frame transformation to decouple the 3-phase measured inverter current (I_{abc}^*) into quadrature and direct components, which can be independently tuned to

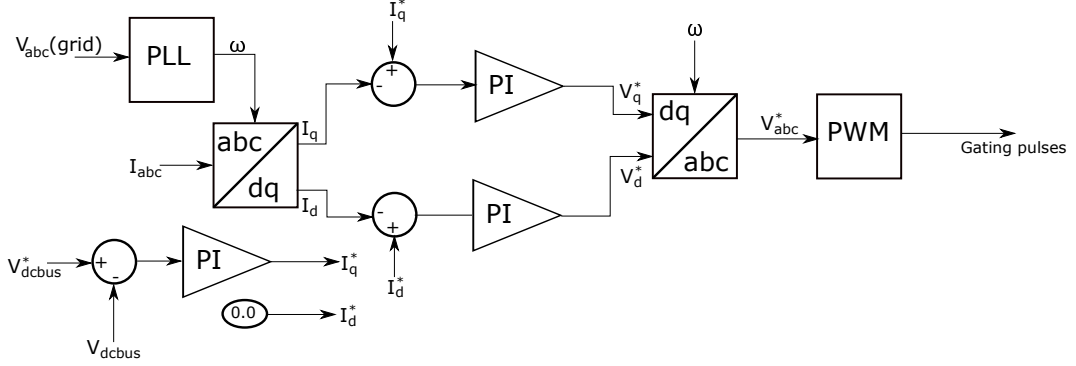


Figure 3.6: Grid side inverter control diagram. The control maintains I_d at zero so that the inverter neither absorbs nor supply reactive power while I_q is used to regulate the real power output by keeping the bus voltage constant at a reference value.

control active and reactive power flow into the grid respectively . In PSCAD, V_d is configured to control the flow of reactive power while V_q controls the real power output. Since all the simulations in this research were done on active power control only, I_d^* is kept at zero so that the PV system operates at unity power factor. I_q^* is proportional to the amount of real power the PV system needs to supply in order to maintain the DC bus voltage at the reference value (V_{dcbus}^*). V_d^* and V_q^* are then transformed with the grid phase angle to produce the reference voltage waveform (V_{abc}^*) used to generate the PWM pulses.

3.4 BESS

The battery is connected to the grid through its own inverter as shown in Fig. 3.1, since BESS units are usually deployed at a separate locations from the PV system. Battery energy storage systems have been primarily used for frequency regulation and

load shedding applications as described in [63]. In this approach, the BESS is only used for real power transfer. The battery discharges power to the grid to supply the power deficit from the PV if its SOC is above minimum, and charges from the grid when the PV array is producing excess power with battery SOC is below maximum [64]. The modeled battery side inverter has a grid voltage oriented control similar to that of the PV array. In this case, the active current reference (I_{qref}^*) is controlled such that the summation of the PV system (P_{pv}) and battery (P_b) real power output is maintained at a specified reference value (P_{ref}^*) and the reactive current component (I_{dref}^*) is used to ensure that the reactive power (Q_b) output is maintained at its reference value (Q_{ref}^*),

$$I_{qref}^* = [P_{ref} - (P_{pv} + P_b)] * \left(K_p + \frac{1}{K_i} \right), \quad (3.2)$$

$$I_{dref}^* = (Q_{ref} - Q_b) * \left(K_p + \frac{1}{K_i} \right). \quad (3.3)$$

The 3-phase current from the battery inverter is transformed to the d-q frame where the q-axis and d-axis current components are used to control the active power and reactive power flow respectively. The PI controller for battery discharge current is used to ensure that the sum of the real power produced by the battery and PV is maintained at a specified reference value as shown in Fig. 3.7, such that the battery only supplies the amount of real power lost during shading of the PV panels as long

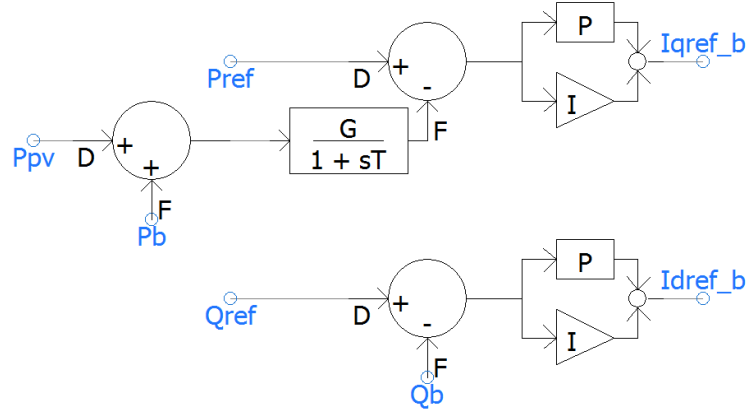


Figure 3.7: Control diagram for BESS reference current components. $I_{qbre f}$ and $I_{dbre f}$ are fed to an inner controller to generate voltage reference, which is subsequently used to produce inverter gating signals.

as the terminal voltage of the battery is above the battery voltage that represents the minimum state of charge. While the PI controller for charging produces a negative real power current reference corresponding to the amount of power required to increase the battery terminal voltage to a value that represents the maximum state of charge. The reactive power reference ($I_{dref b}^*$) for this design was maintained at zero so that the battery does not supply reactive power, this component can also be varied such that the battery inverter compensates for the inductive loads in the system.

3.5 Modified IEEE 14 Bus Test System

The IEEE 14 bus system represents a portion of the American electric power system in the Midwestern US, which is widely accepted by researchers to implement

new ideas and concepts in power system engineering related to short circuit analysis, load flow studies, and grid interconnection problems [65]. The system consists of 14 buses, 11 loads and 5 generators of which 3 are synchronous condensers and one slack bus. The Manitoba HVDC research center model of the IEEE 14 bus system, which has the parameters listed in Table 3.4 was adopted in the current study.

In the modified IEEE 14 bus system, the 3-phase voltage supply at bus no. 2 is replaced with the designed 10MW PV system connected in parallel to a 100MVA synchronous generator as shown in Fig. 3.8 [7]. Since the PV power rating is only a fraction of the generator ratings, the PV and generator will supply the total amount of power needed by the connected load. In a case of complete shading of the PV array the parallel synchronous generator steps up its output power to supply the connected loads when the battery has a state of charge below minimum. This system can also be integrated such that the PV supplies all the power required by the loads connected to the bus, in such design the PV system will solely supply its rated power during the day, At night when the PV system is not supplying power, automatic generator control is used to divide the load among the connected generators for optimum economic dispatch.

Table 3.3: Transmission line characteristics of IEEE 14-bus system [7].

Line		R [pu/m]	X [pu/m]	B [pu/m]
from bus	to bus			
1	2	1.94E-07	5.92E-07	5.28E-07
1	5	5.40E-07	2.23E-06	4.92E-07
2	3	4.70E-07	1.98E-06	4.38E-07
2	4	5.81E-07	1.76E-06	3.40E-07
2	5	5.70E-07	1.74E-06	3.46E-07
3	4	6.70E-07	1.71E-06	1.28E-07
4	5	1.34E-07	4.21E-07	1.00E-09
6	11	9.50E-07	1.99E-06	1.00E-09
6	12	1.23E-06	2.56E-06	1.00E-09
6	13	6.62E-07	1.30E-06	1.00E-09
7	8	1.00E-09	1.76E-06	1.00E-09
7	9	1.00E-09	1.10E-06	1.00E-09
9	10	3.18E-07	8.45E-07	1.00E-09
9	14	1.27E-06	2.70E-06	1.00E-09
10	11	8.21E-07	1.92E-06	1.00E-09
12	13	2.21E-06	2.00E-06	1.00E-09
13	14	1.71E-06	3.48E-06	1.00E-09

Table 3.4: Load characteristics of IEEE 14-bus system [7].

Bus	P [pu]	Q [pu]
2	0.217	0.127
3	0.942	0.190
4	0.478	-0.039
5	0.076	0.016
6	0.112	0.075
9	0.295	0.166
10	0.090	0.058
11	0.035	0.018
12	0.061	0.016
13	0.135	0.058
14	0.149	0.050

3.6 Simulation Results and Discussion

A single unit of the PV system with BESS is modeled and simulated in PSCAD environment as illustrated in Fig. 3.2 with a simulation time step of $5\mu s$. In this scenario, the PV inverter maintains the DC bus voltage at 0.6kV (Fig. 3.12) while transferring the PV array power to the grid at unity power factor (Fig. 3.10). Battery energy storage system is used to limit the output power of the system at 0.7MW, making it charge when the PV array power is above reference and discharge when below. At 12s simulation time the PV array is suddenly shaded and its irradiance is reduced from $1000W/m^2$ to $500W/m^2$ for 10s to illustrate a passing cloud. The change in PV array irradiance leads to a sudden decrease in the DC bus voltage following which, the PV inverter reduces its real power reference current component to compensate for the shading and vice versa for the increase in irradiance (Fig. 3.13). When the PV array is suddenly shaded, the array terminal voltage sharply moves away from the MPP before the MPPT controller adjusts its duty ratio so that the array is back at MPP (Fig. 3.9 and 3.11).

To simulate the relationship of the entire system with the grid, multiple units connected in parallel were connected to the IEEE 14 bus no. 2 (Fig 3.8). At 15s simulation time, the PV array irradiance is suddenly reduce from $1000W/m^2$ to 0 leading to a transient reduction in the bus frequency (Fig. 3.20) before the adjacent synchronous generator steps up its real power output to supply the power deficit from

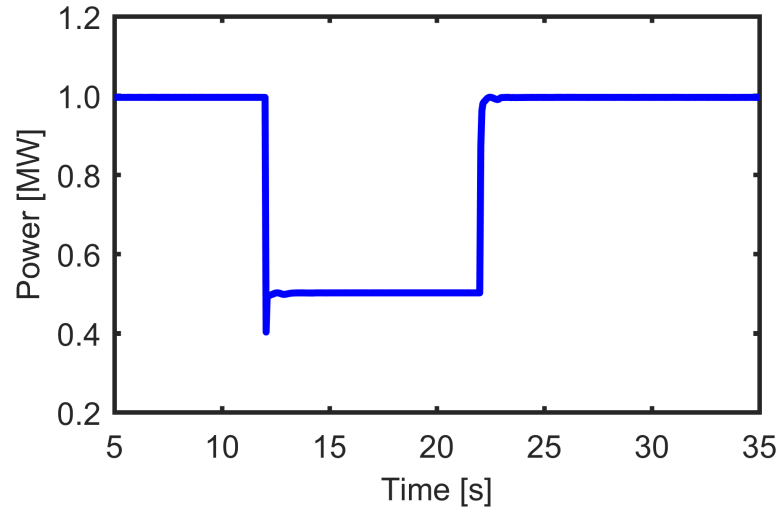


Figure 3.9: PV DC Power. Reduction in irradiance leads to decrease in PV output current making the PV DC power alternate with respect to changes in irradiance.

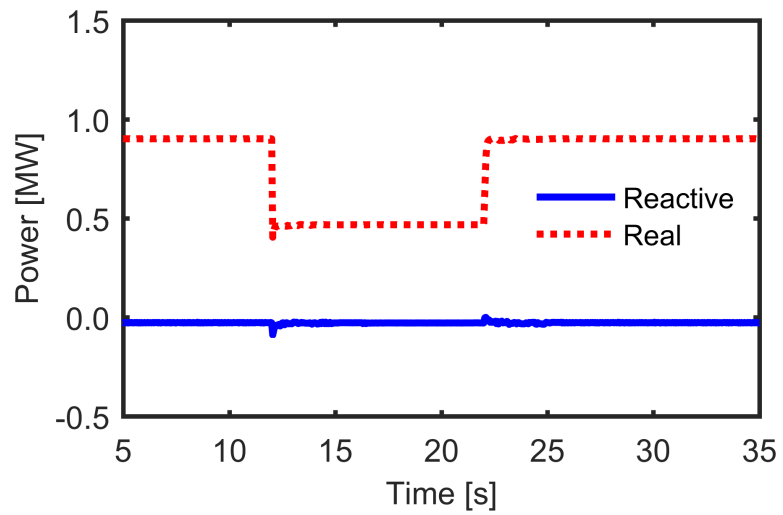


Figure 3.10: PV AC power output at unity power factor irrespective of changes in array irradiance.

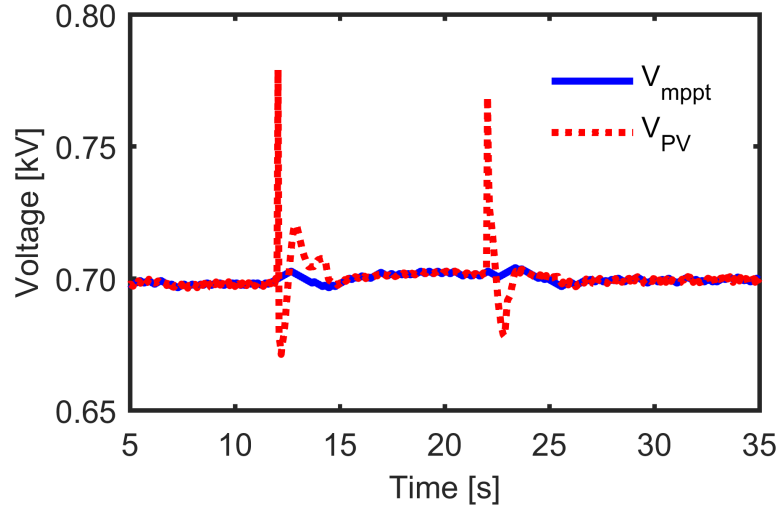


Figure 3.11: PV array MPPT reference and terminal voltage. With changes in irradiance, DC-DC converter ensures that the PV array still operates at MPPT.

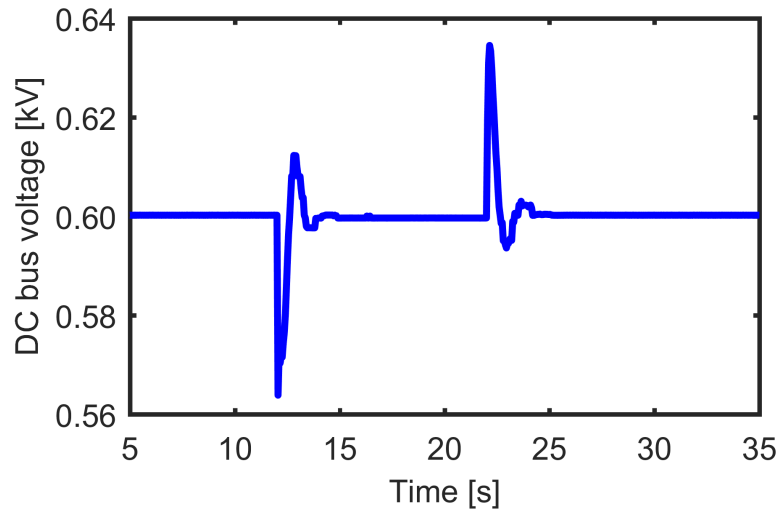


Figure 3.12: The control loop maintains the DC link voltage at 0.6kV by regulating the q-axis current component.

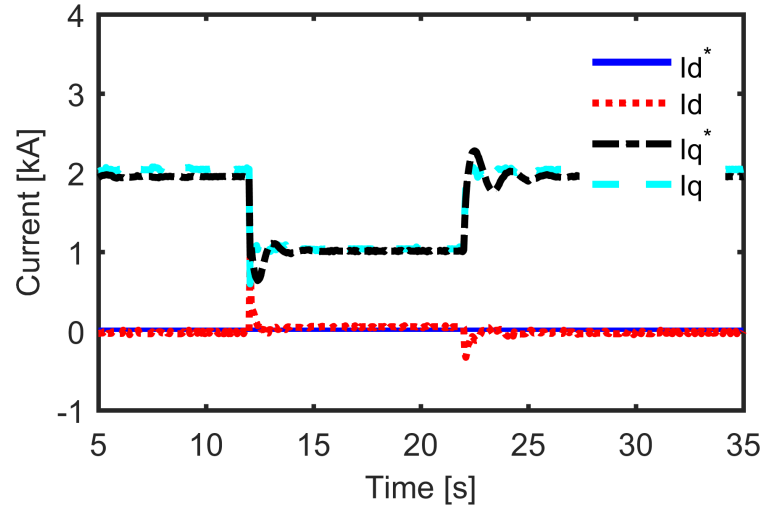


Figure 3.13: Inverter actual and reference current components. I_d^* is maintained at 0 so that reactive current component is zero and I_q^* is regulated to maintain the PV DC bus voltage at reference value

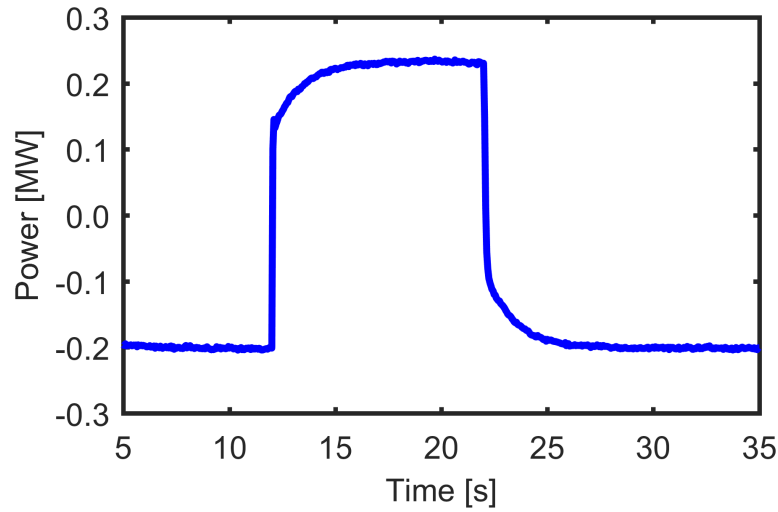


Figure 3.14: BESS real power output. At 1000W/m^2 the PV system is supplying excess power allowing the BESS to charge, when array is suddenly shaded, BESS changes from charging to discharging mode to supply the power deficit.

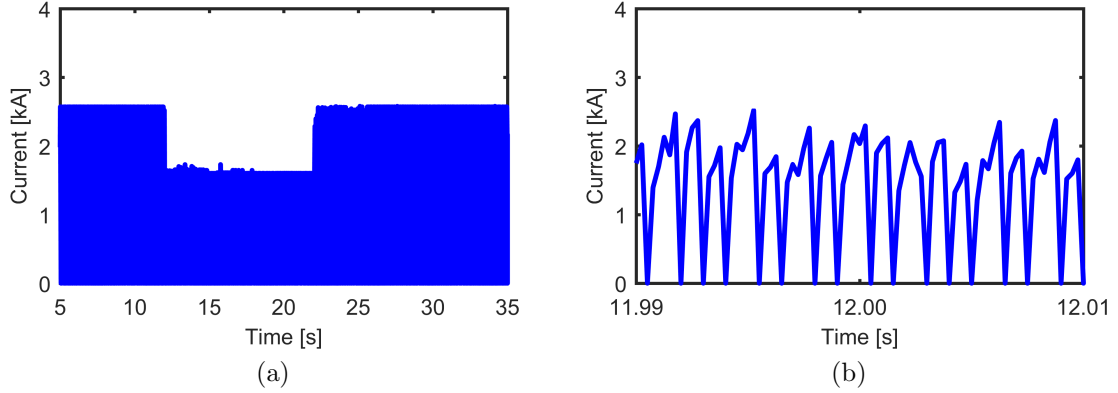


Figure 3.15: (a) Inverter input current and, (b) zoomed representation. The inverter input current is discontinuous due to high frequency switching of inverter switches and its maximum current reduces with decrease in the amount of PV irradiance

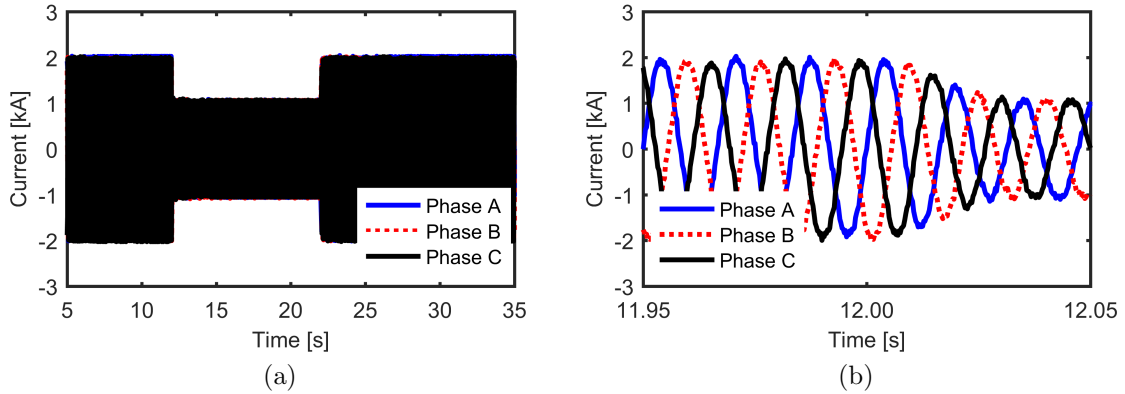


Figure 3.16: (a) PV system output current and, (b) zoomed representation . When PV array irradiance reduces, I_q^* reduces so that DC link voltage is maintained at reference value.

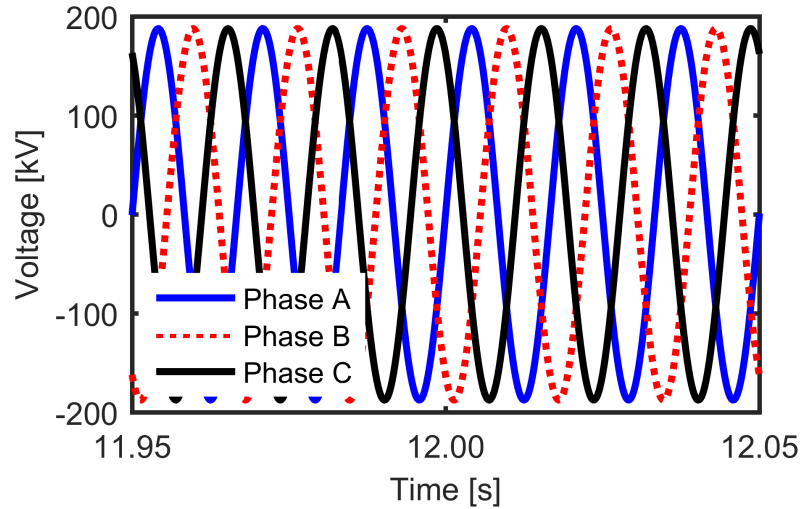


Figure 3.17: Grid voltage. Grid voltage is maintained constant with changes in PV irradiance.

the PV and maintain the bus voltage at reference value of 60Hz (Fig. 3.21). In this case, the adjacent synchronous generator can comfortably supply the power deficit since its rated for 100MW while the PV system is rated for 10MW.

3.7 Summary

This chapter discusses the layout of a multi-megawatt grid connected battery integrated PV system connected to the standard IEEE 14 bus with the entire model built in PSCAD, which is a tool typically employed for power system transient analysis. The system consists of several sections, each with their own PV array, DC-DC and DC-AC converters. These sections are connected in parallel. The inverters of adjacent sections may be connected in cascade to obtain a multilevel voltage waveform,

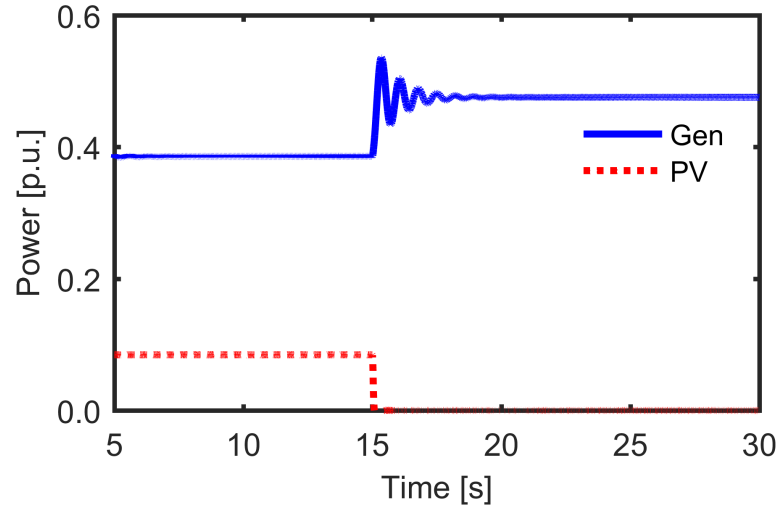


Figure 3.18: PV system and synchronous generator real power output ($S_{base} = 100\text{MW}$). Adjacent synchronous generator increases its turbine mechanical power to supply power lost from PV.

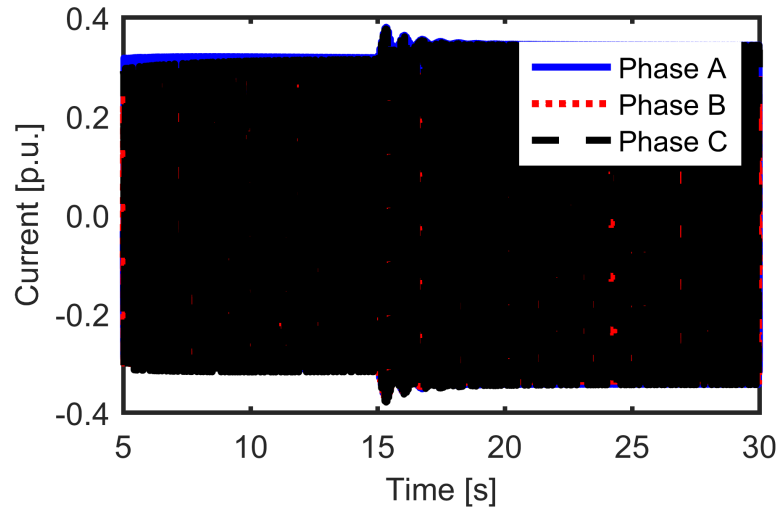


Figure 3.19: Generator output current increases when PV is being shaded to supply the power deficit.

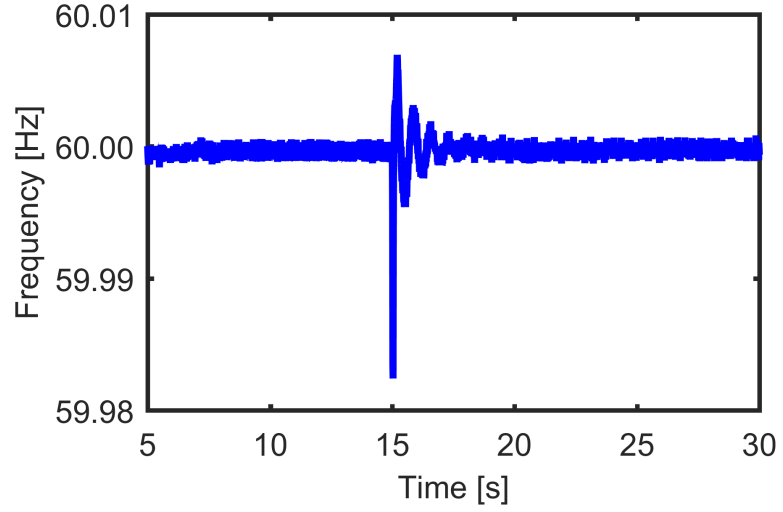


Figure 3.20: Modified IEEE 14 bus no 2 frequency. The sudden loss of PV power leads to a transient in the bus voltage frequency before the generator power increases to supply the power deficit and maintain the frequency at 60Hz.

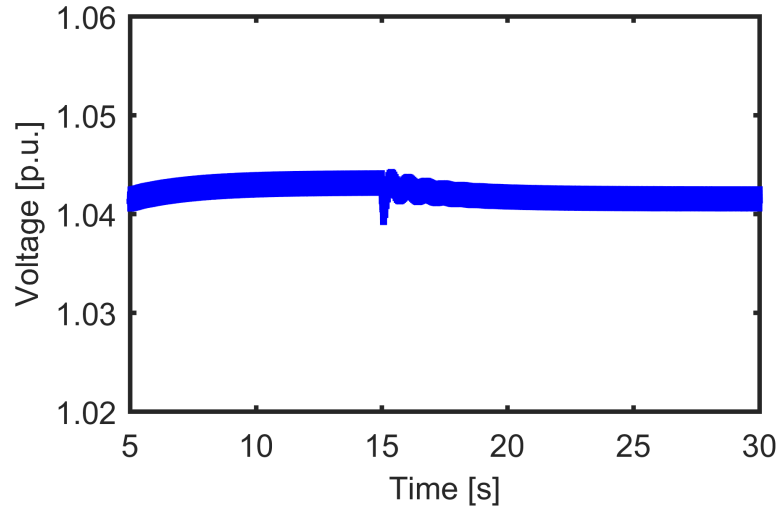


Figure 3.21: Bus no 2 RMS voltage. The bus voltage is maintained within acceptable limit throughout the transient ($V_{base} = 138\text{kV}$).

thereby reducing the filter requirement. Grid voltage oriented control is used for the grid side inverters, allowing independent control of active and reactive power. The battery is connected to the grid via its own inverter. It is controlled to supply power to the grid when the PV panel is shaded.

Chapter 4

Solar PV Pumping System with Capacity Modulation and Battery Voltage Support

This chapter introduces a method of expanding the capacity of an existing irrigation farm with additional pumps powered by photovoltaics and a method of achieving capacity modulation with the multiple pumps connected to the PV system by energizing the minimum amount of pumps required to meet a particular load demand.

4.1 Introduction

Investment in renewable energy is increasing with the advent of global warming. Solar energy seems to be the most attractive form of renewable energy since it can meet most power requirements and is scalable from small residential to multi-MW installations. Pumping systems are generally employed for fluid distribution in both

large-scale and small-scale farm irrigation systems and companies including World-Water & Solar Technologies Corp. have invested in the use of multi-megawatt PV system to power large irrigation farm systems [66]. Since the amount of water required by agricultural crops varies depending on the season of the year where summer sees the largest, irrigation pumping system are rarely operated at full capacity.

Some of the literature existing regarding PV and pumping systems have focused on the method used for maximum power point tracking (MPPT) and the type of DC-DC converter used for the tracking [67–71]. Authors of [72, 73] propose the use of DC pumps connected to the PV array to eliminate the use of an inverter, some powered the pumps using induction motors [74–78] and brushless DC motors (BLDC). Different control strategies have been proposed for the control of the connected motors [79–86]. The DC link voltage of the connected BLDC motor was varied in order to regulate the pump speed in [87] and, [75, 88] proposed a drive for a 2-phase induction motor. The increased operation and maintenance cost due to the presence of commutator and brush gears has been the major disadvantage of DC motors connected to PV systems [89].

The proposed system consists of multiple permanent magnet synchronous motor (PMSM) driven pumps connected in parallel to a common DC bus through speed controlled voltages source inverter(VSI), these pumps are primarily energized by an array of PV modules connected to the common DC bus through a DC-DC converter

used for MPPT. A BESS is connected to the DC bus for voltage support and to ensure system stability when the power required by the pump at a reference speed is more than the power available from the PV array. The grid is connected to the DC bus through a bidirectional AC-DC converter used to supply power to the pumps when the battery state of charge is below the minimum and supplies excess power to the grid when battery state of charge (SOC) is above the maximum. To achieve capacity modulation similar to that of air conditioning system introduced in [90], only the minimum amount of pumps required to meet a specified load demand are energized instead of having all pumps operate at fractions of the rated power. This chapter introduces a method of connecting multiple pumping system for capacity modulation to a multi-megawatt PV system with battery voltage support and possible grid interconnection.

4.2 System Configuration

The block diagram describing how an array of PMSM driven pumps connected in parallel are interfaced via a DC-AC converter to a common DC bus energized by a combination of PV array, BESS and the grid is shown in Fig. 4.1. This system can be operated in different modes: (1) When the amount of power from the PV is sufficient to energize all the pumps required for operation, the BESS and the grid are isolated from the DC link, (2) When the PV power is insufficient to energize

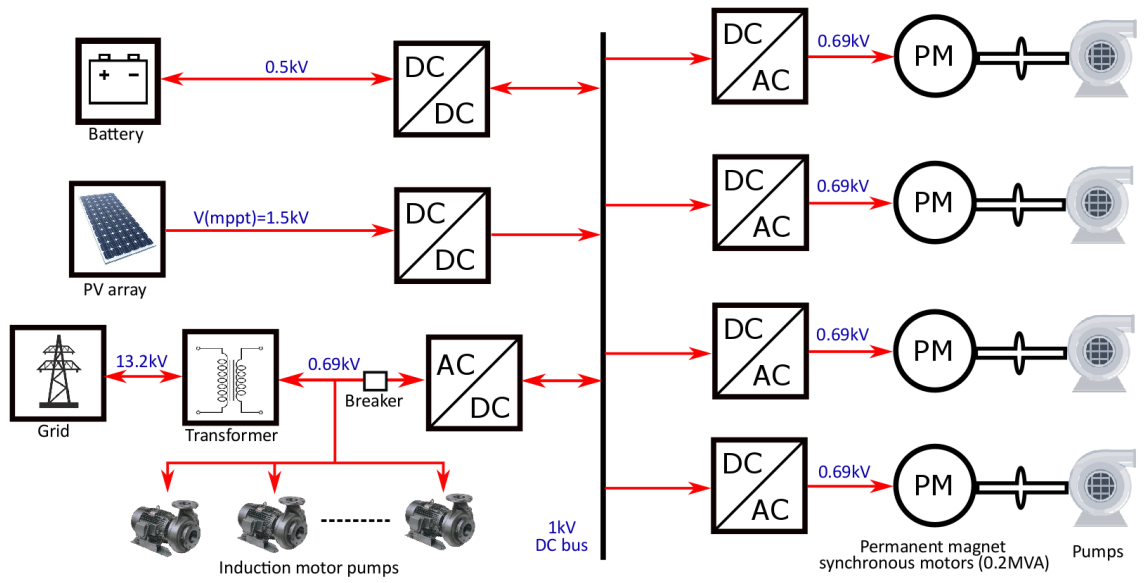


Figure 4.1: System overview showing how existing pumping system connected to the grid can be expanded with multiple PMSM driven pumps for capacity modulation powered by solar PV. The grid in this system is used to maintain DC bus when battery is unavailable due to SOC constraints and $V(\text{mmpt})$ is the MPPT voltage at $1000\text{W}/\text{m}^2$ with 25°C cell temperature

the required pumps, deficit power is absorbed from the BESS if its SOC is above minimum otherwise the needed power is taken from the grid, (3) When PV power is excess, the battery charges from the DC bus if its state of charge is below maximum otherwise, the excess power is transferred to the grid.

4.2.1 PV array

The PV cell model provided in PSCADTM/EMTDCTM is based on the Norton equivalent circuit which is one of many PV equivalent circuit models. The output current (I) of the PV array is given in Equation 3.1.

In order to meet power electronics conditioning requirements, PV modules are typically connected in series so their individual voltages add up. In this design, the PV array is made up of 40 PV modules connected in series and 80 module strings in parallel. Each PV module is designed to have an open circuit voltage of 46.75V and short circuit current of 9.04A. At 1000W/m² solar irradiance and 25°C cell temperature, each module is capable of providing maximum DC power of 316.5W at 37.4V terminal voltage. To increase the PV system capacity, multiple PV array can be connected in parallel via individual DC-DC converter for MPPT to the DC bus [91].

4.2.2 BESS

When the amount of power required by the connected pumps is above the power from PV array, the inverter control reaches an unstable condition if BESS is absent,

since the q-axis reference current component (i_q^*) keeps increasing till the DC link is short-circuited. In this approach, the BESS whose terminal voltage is 0.5kV maintains the DC link voltage at reference value (1kV) by supplying the power deficit or absorbing excess power from the PV via DC-DC converter. The output voltage of the battery model used in PSCAD is described in (4.1).

$$E = E_0 - K \cdot \frac{1}{SOC} + A \cdot e^{-B \cdot Q(1-SOC)}, \quad (4.1)$$

where E is no-load voltage, E_0 is battery constant voltage, K is polarization voltage, Q is battery capacity, A is exponential zone amplitude, B is exponential zone time constant inverse and SOC is the battery state of charge.

4.2.3 Pump system

The induction motor pumps directly connected to the grid represents the existing pumping system used to meet the base load while the PMSM driven pumps with variable speed control, energized by the PV system are the pumps used for expanding the capacity of the irrigation farm. Each PMSM is rated for 0.2MVA, 0.69kV at 60Hz and modeled such that the per unit load torque is the square of the per unit operating speed so it represents a pump. The voltage equations for the main stator windings of the machine in the dq0 reference frame is given in Equation (2.15). The multiple pumps can also be replaced by a single pump to achieve capacity modulation through reference speed variation of the high power rated pump which might be complex and

expensive to design since it requires high efficiency over all speed.

4.3 Design Considerations

This system proposes a method for 100% capacity expansion of an irrigation farm pumping system. It is common to use multiple pumps in large farm irrigation pumping system for reachability, multiple access point to underground water, reliability and ease during maintenance. Also, a complex layout is required to design a single high rated pump with a flat efficiency over all speeds. Multiple inverters are used to achieve independent control of each pumps using a rotor positioning device embedded in the PMSM. The connected pumps are rated for 0.2MVA each with 0.69kV rated line to line voltage (V_{LL}). The minimum DC link voltage (V_{DC}) is calculated using:

$$V_{DC} = \frac{3\sqrt{2}}{\pi} V_{LL} = 1.351 * 690V = 932.19V, \quad (4.2)$$

since the minimum DC link voltage is 932.19, the system is designed with a DC link reference of 1kV.

In a system where the PV array is directly connected to the pump inverter without a DC-DC converter, the system fails to operate when the power available from the PV is lower than the power required by the load if the reference active current component(I_q^*) is obtained from the speed loop. This is because I_q^* keeps increasing so the pump operates at reference, which forces the PV array to supply its maximum current at zero voltage (short-circuit). With DC-DC converter for MPPT, the

PV array output is maintained at MPP irrespective of the current demand of the pump. Instead, I_q^* reference becomes saturated making the current non-sinusoidal and produces and unstable torque.

Variable solution time step solvers have the ability to automatically use large time-steps for small frequency signals and small time-step for high frequency signals. The PSCADTM/EMTDCTM software on the other hand utilizes a constant time step solver, which uses constant time-step throughout its entire simulation and interpolates the system response in between time-steps, making it less accurate when signal's frequency is greater than the solver's frequency. To increase the simulation accuracy solution time-step smaller whose frequency is greater than the highest frequency response in the system was chosen.

4.4 Proposed System Control

4.4.1 DC-DC converters

Increase in solar irradiance leads to increase in output current of a PV module while increasing its cell temperature decreases its output voltage. The maximum available power of a PV depends on its electrical properties and the atmospheric condition at the installation location while the operating point depends on the load connected to it. In order to ensure that the system PV array is constantly operating at its maximum power point (MPP), a buck converter is used to vary the magnitude

of the impedance seen by the PV so it operates at its MPP. In this design, The PSCADTM/EMTDCTM MPPT block, which is designed based on the incremental conductance method is used to determine the voltage that corresponds to the MPP voltage (V_{mppt}), then a PI controller is used to regulate the duty cycle of the converter switch so that the PV output voltage is equal to V_{mppt} . In order to maintain the DC bus voltage at a constant value of 1kV, the 0.5kV battery is connected to it through a half-bridge bidirectional DC-DC converter, which can either be operated as a boost converter to discharge the battery when the DC bus voltage is below reference and the battery SOC is above minimum or operated as a buck converter to charge the battery when the DC bus voltage is above reference and the battery SOC is below maximum.

4.4.2 DC-AC converters

The PMSM driven pumps are connected to the DC bus through a VSI operating in speed control mode. The reference d-axis and q-axis pump current components (I_d^* & I_q^*) are transformed to *abc* domain using the rotor position as the transformation angle to generate the reference 3-phase current (I_{abc}^*), which is compared with the actual 3-phase pump current (I_{abc}) by the hysteresis current controller (HCC) to produce the gating signals for the inverter switches (Fig. 4.3).

The grid connected bidirectional inverter maintains the DC bus voltage when

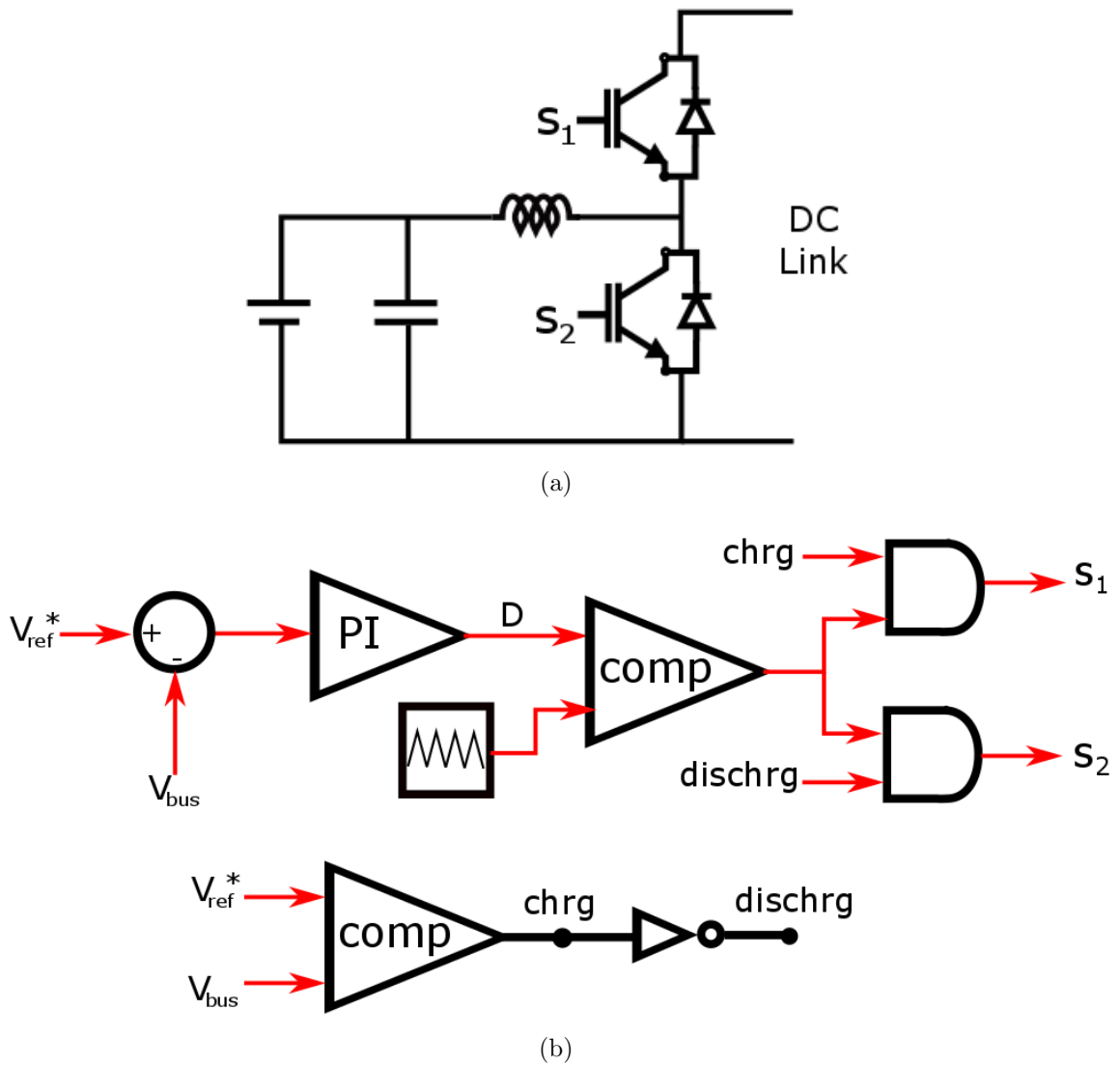


Figure 4.2: (a) BESS connected to the DC bus through DC-DC converter where switch S_1 is used to regulate the charge current and S_2 controls the discharge current, (b) BESS converter control so that battery supplies the amount of current required to keep DC link voltage at reference value

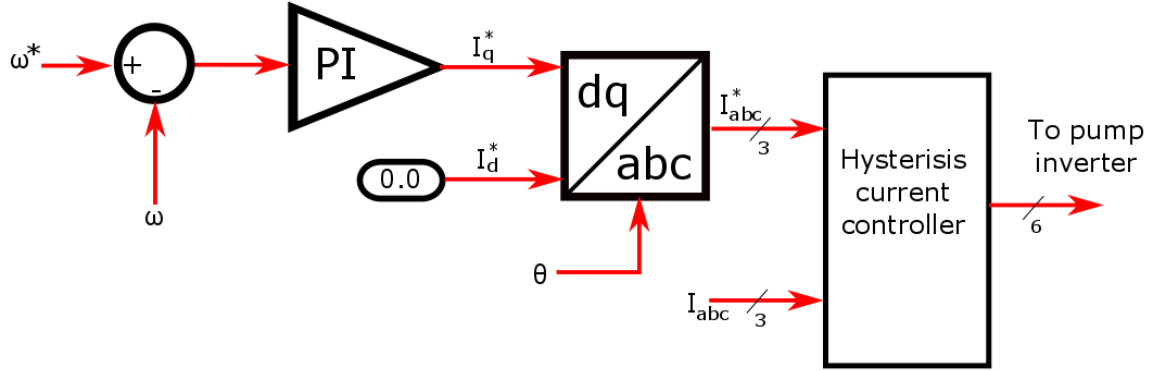


Figure 4.3: PMSM inverter control

the battery is unavailable due to SOC constraints. The q-axis and d-axis current components are used to control the active and reactive power flow respectively. When the battery SOC is below minimum and the DC link voltage is below reference, the breaker is closed and the grid connected inverter absorbs real power from the grid to return the bus voltage to its reference value or absorb excess power from the PV array through the common DC bus to maintain the DC link voltage at the reference value when the battery SOC is above maximum while the bus voltage is above reference. The grid connected inverter can also be used to supply reactive power to the grid at night when the PV array is completely shaded and the connected pumps are not being operated.

4.4.3 Capacity modulation

Just like compressor modulation for air conditioning system, the amount of energized pumps in an irrigation system can be modulated such that only the minimum

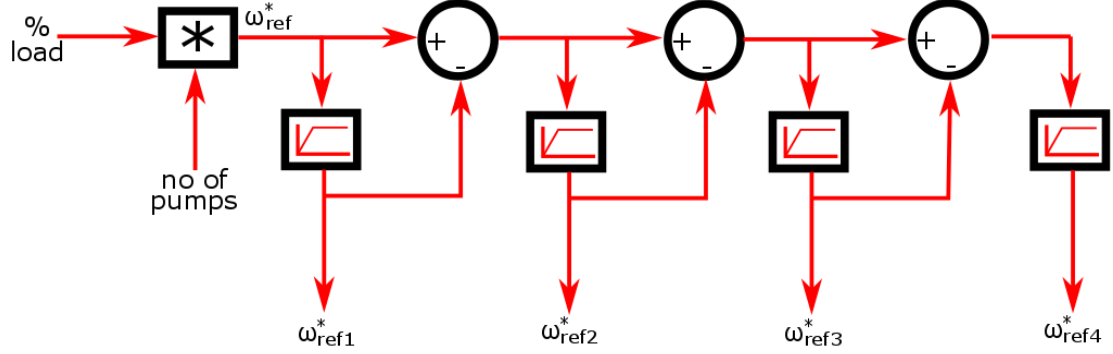


Figure 4.4: Capacity modulation control

amount of pumps required to meet a specified load demand are energized. In this design, the percentage load required is multiplied by the number of pumps to be modulated for w_{ref} , which is then connected to pump 1 reference speed (w_{ref1}) and saturated at 1pu. The difference between w_{ref} and w_{ref1} is connected to w_{ref2} through a 1pu saturation block and the difference is also passed to other pumps (Fig. 4.4). Another method of capacity modulation can be achieved with the minimum amount of pumps all operated at the same average speed.

4.5 Simulation Results and Discussion

The performance of the proposed system was designed and simulated at $10\mu s$ solution time-step using PSCADTM/ EMTDCTM, with the HCC switching at about 3kHz. The operation of the proposed system was first tested for speed control with a single pump rated for 0.8MVA instead of the proposed multiple pumps. In this

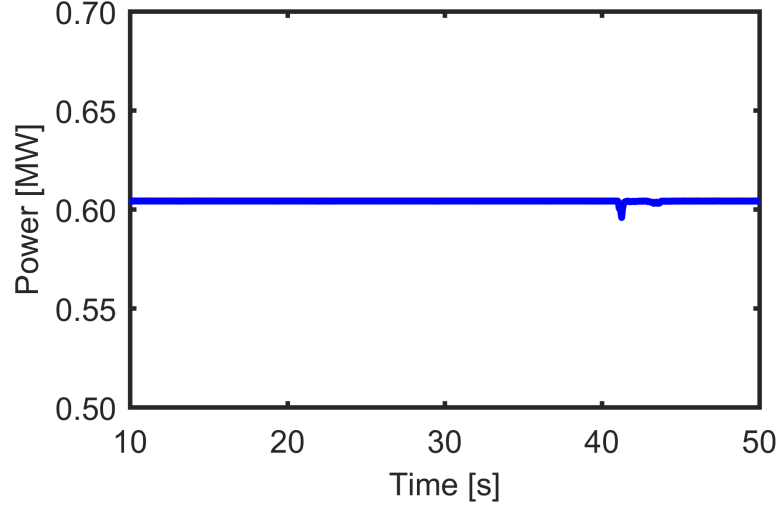


Figure 4.5: PV array DC output power. PV array operates at MPP until battery switches from charging to discharging mode at 40s leading to transient in MPPT computation.

configuration, the reference speed of the pump was varied from 0.25 to 0.5, 0.75 and 1p.u. at 20, 30 and 40s simulation time respectively. The PV irradiance was maintained at $600\text{W}/\text{m}^2$ throughout the simulation making the PV array DC output power almost constant (Fig. 4.5). At 40s, the power required to maintain the pump at the reference speed is more than the PV array can provide, which makes the DC link voltage reduce below reference (Fig. 4.6) leading to the battery going from charging to discharge mode to supply the power deficit and return the DC link voltage to its reference (Fig. 4.7). Other parameters are observed in Fig. 4.8, 4.9, 4.10, 4.11 and 4.13.

It is impossible to have a constant level of irradiance over a long period of time. Based on the irradiance data collected from [1] and [92], the maximum change in

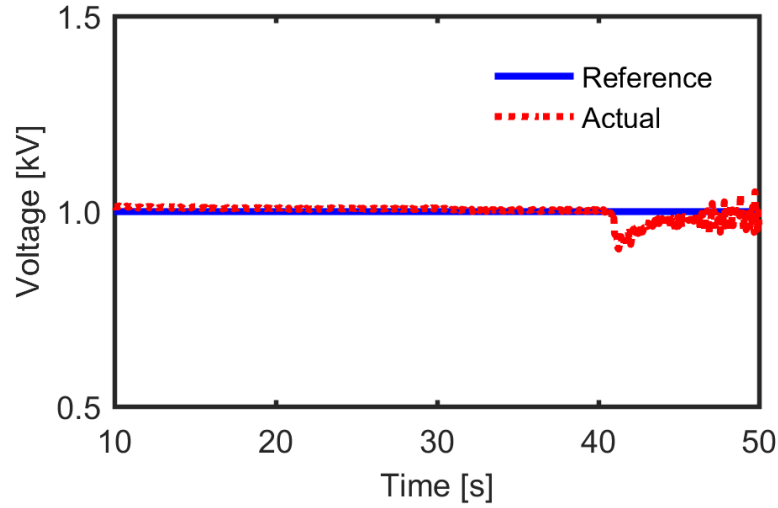


Figure 4.6: DC bus voltage. At 40s simulation time, power required to energize the pump at reference speed is greater than power from the PV array, which lead to drop in bus voltage before the battery starts to discharge.

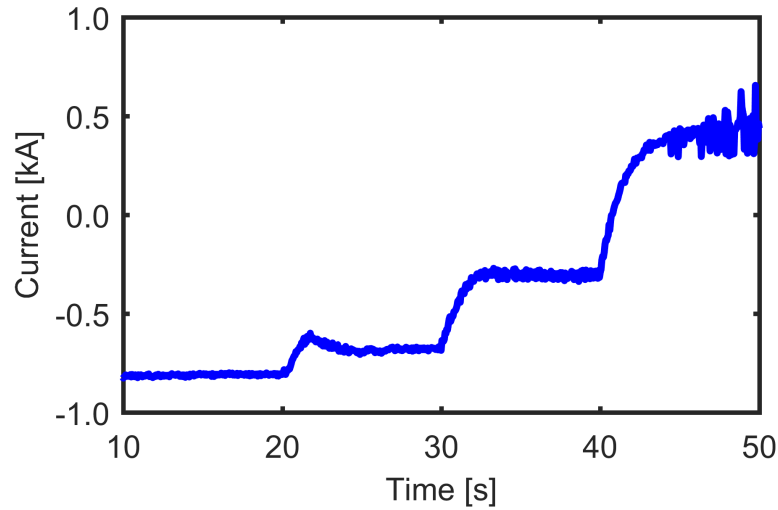


Figure 4.7: Battery output current. Battery absorbs the excess energy from the PV array to maintain the DC link bus voltage at 1kV and supplies power to the DC link at 40s when the bus voltage is below reference.

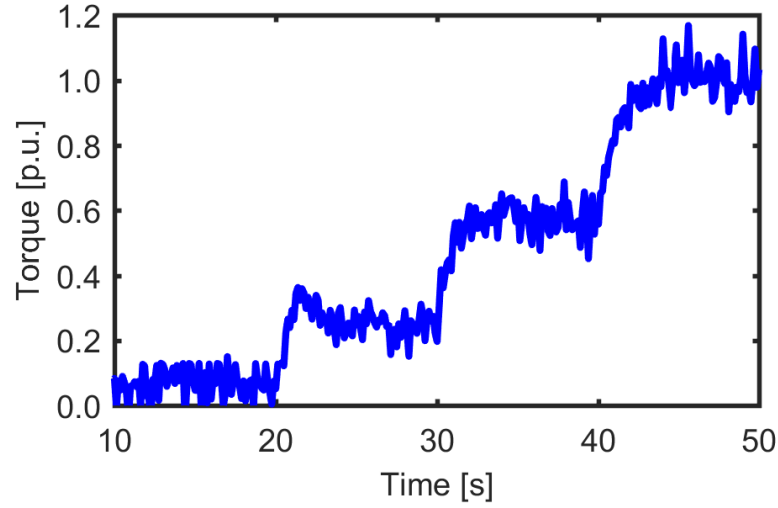


Figure 4.8: Pump torque. With increase in PV reference speed, PMSM torque increases corresponding to the square of the reference speed

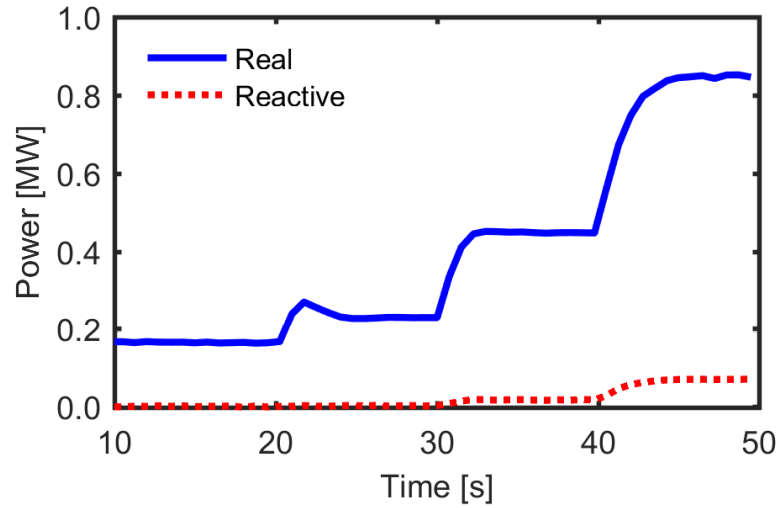


Figure 4.9: Pump reactive and real power intake. The single PMSM pump connected to the system is rated for 0.8MVA and absorbs real and reactive power sufficient to keep it operating at the reference speed with maximum torque.

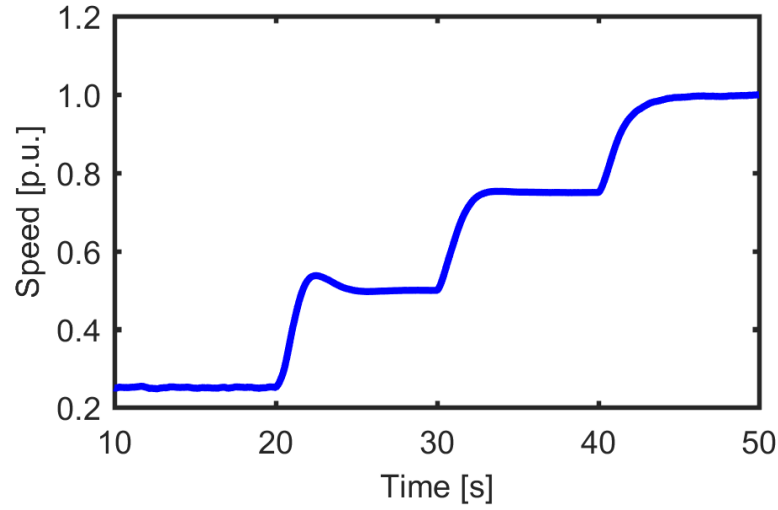


Figure 4.10: PMSM speed. With increase in load demand, PMSM inverter adjust to increase the pump speed

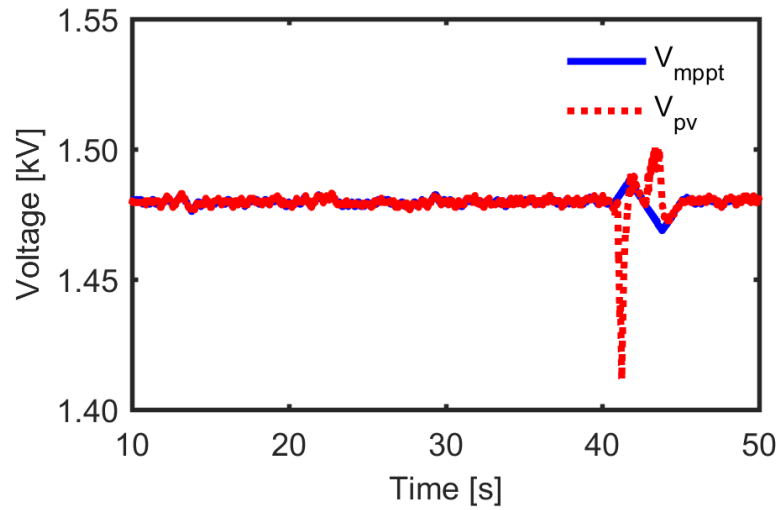


Figure 4.11: MPPT reference and PV array output voltage. At 40s when the battery changes from discharging to charging mode, the MPPT adjust its reference so the PV remains at its MPP

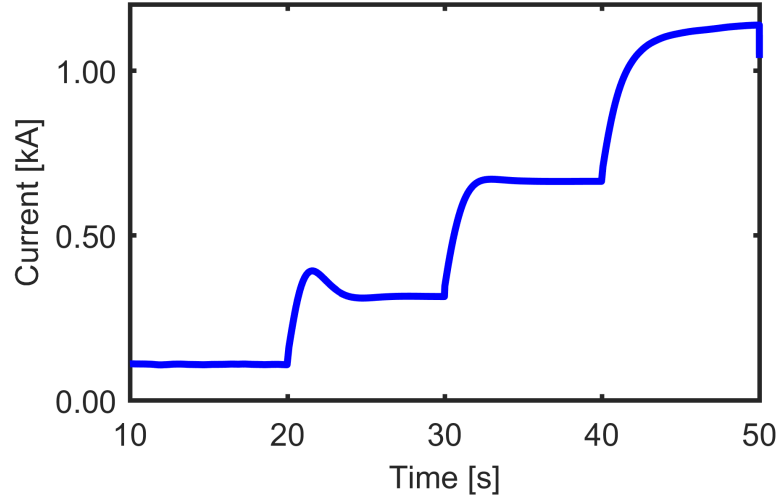


Figure 4.12: Pump inverter reference active current component. In order to increase the pump speed, the reference active current component (I_q^*) is also increase.

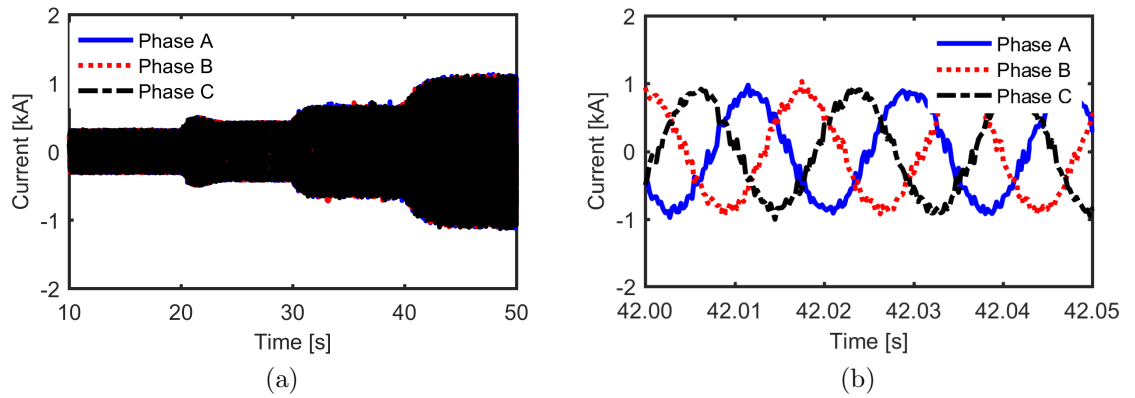


Figure 4.13: (a) Pump current and, (b) zoomed representation. With increase in speed reference, the pump absorbs more current to meet the load demand.

the irradiance recorded over a period of 5min is below $200\text{W}/\text{m}^2$. To illustrate the worst case scenario, the performance of the PV system is observed when the PV array is suddenly shaded from $1000\text{W}/\text{m}^2$ to $500\text{W}/\text{m}^2$ at 7s simulation time for 8s while the pumps are modulated for 80% load capacity. At $1000\text{W}/\text{m}^2$, the PV array is producing excess amount of power while the battery charges to maintain the DC link voltage at 1kV (Fig. 4.15, 4.16). The battery discharges when the PV array irradiance is suddenly reduced to $500\text{W}/\text{m}^2$ in order to supply the additional power required to maintain the DC link voltage at the reference value while the PV operates at its MPP (Fig 4.14).

The operation of the pumps when the percentage load requirement is varied from 25% to 50%, 75%, 80% and 100% is illustrated in Fig. 4.19, 4.18 and 4.17. At 25% load requirement, pump 1 is operated at 1pu speed to meet the load requirement while other pumps remain at zero. With every 25% increase in the load, an additional pump becomes energized to operate at 1pu speed. All connected pumps are operated at 1pu rated speed when the load requirement is 100% while pump 4 operates at 0.2pu speed when the load requirement is 80%.

4.6 Summary

A novel approach for capacity modulation for PMSM driven pumping system powered by PV array with BESS and possibility for grid connection is proposed in this

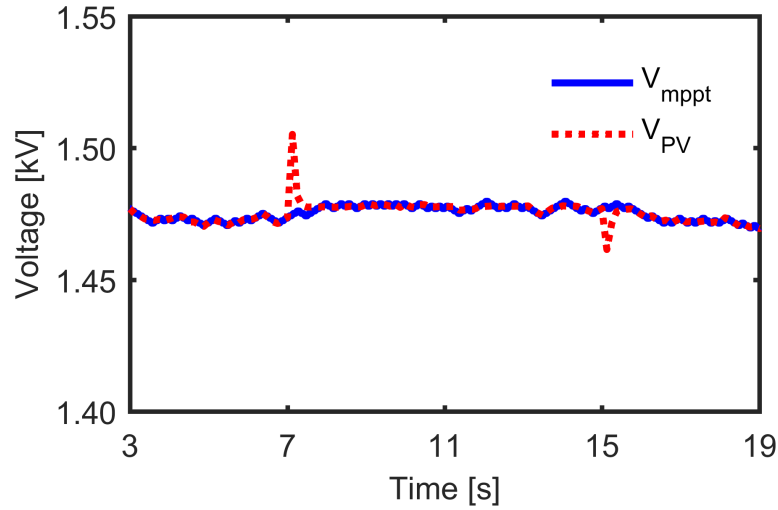


Figure 4.14: Reference MPPT and PV array output voltage when irradiance suddenly drops from 1000W/m^2 to 500W/m^2 at 7s simulation time for 8s making the duty cycle of the DC-DC converter change so that the PV sees a load corresponding to its new maximum power.

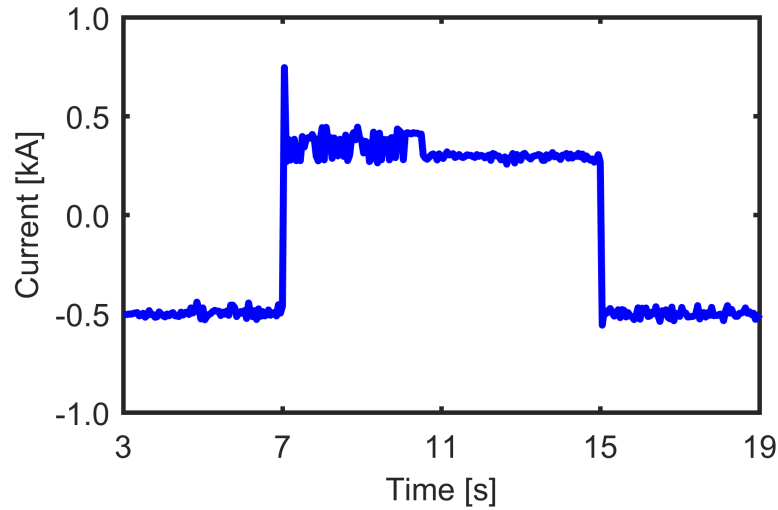


Figure 4.15: Battery output current with change in irradiance effect when the PMSM driven pumps are modulated for 80% load. Irradiance change causes the battery to switch from charging to discharging to supply deficit power required to keep the pumps operating at reference speed.

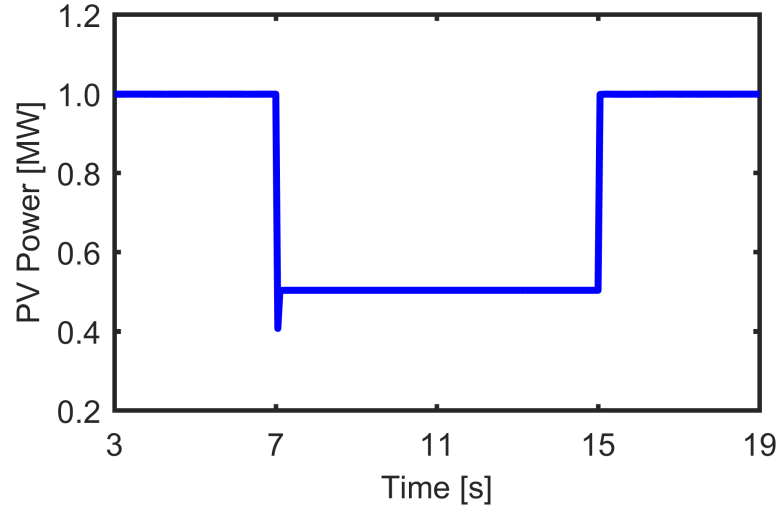


Figure 4.16: DC output power from PV array. When PV array is suddenly shaded, transient effect makes the array slightly move away from its MPP for a short period of time before settling at a new MPP corresponding to the level of solar irradiance.

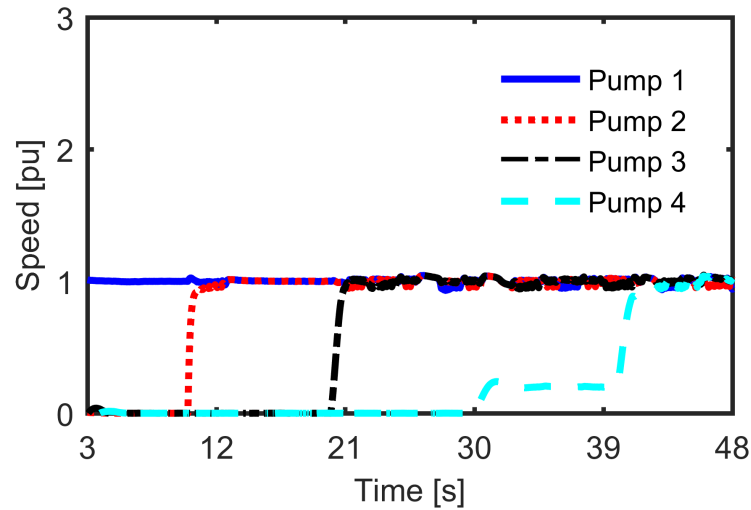


Figure 4.17: Pump speed when reference load changes from 25% to 50%, 75%, 80% and 100% at 10s, 20s, 30s and 40s simulation time respectively making the amount of energized pumps increase to meet speed demand.

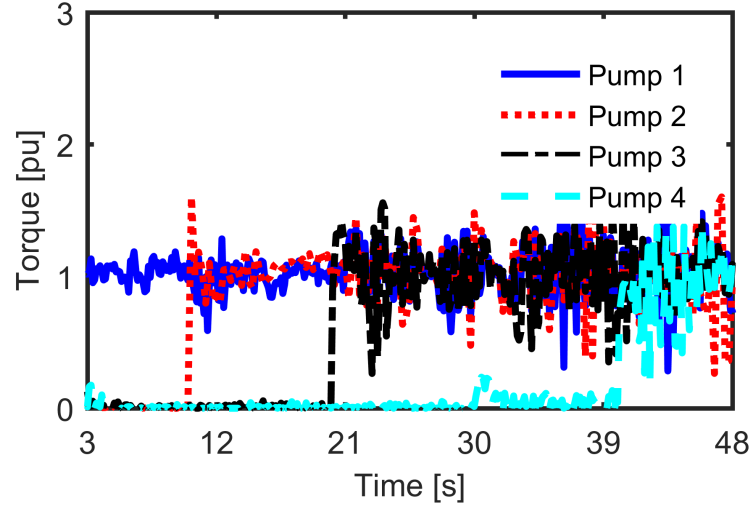


Figure 4.18: Pump electrical torque, which is proportional to the square of the operating speed of each pump.

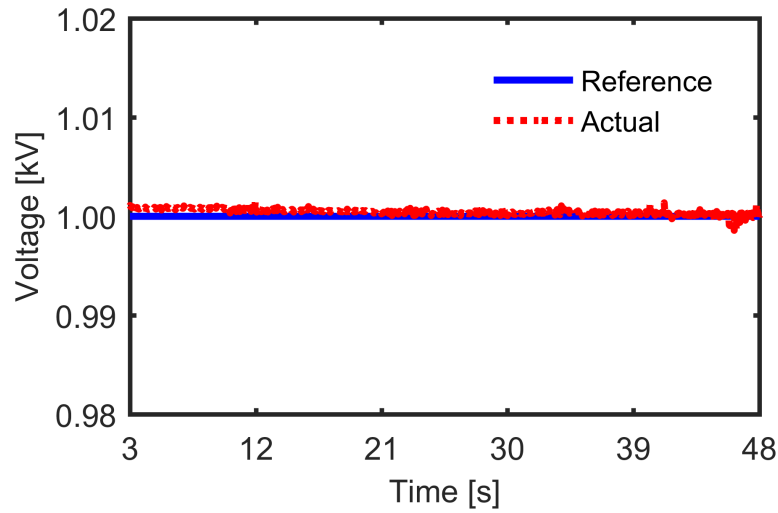


Figure 4.19: DC link and reference voltage. BESS charges and discharge to maintain DC link voltage at reference value even with change in percentage load demand

chapter with focus on method for capacity expansion for an existing irrigation pumping system. The system was designed and simulated in PSCAD/EMTDC environment to test the operation with variation of PV array solar irradiance, load requirement and other parameters. The proposed system is not only able to manage the flow of power from 3 sources to the connected pumps but the DC-AC converter can also be controlled to supply reactive power to the grid when the PV is completely shaded and the pumps are turned off. This system is well suited for rural agricultural usage and allows capacity expansion without dependence on the grid.

Chapter 5

Conclusions and Future Work

5.1 Conclusions

This thesis focused on several methods for integrating battery energy storage system (BESS) with multi-megawatt PV systems. The impact of PV penetration into a modified IEEE 14 bus test system was analyzed. Also, a novel approach for capacity expansion of an existing irrigation farm with pumps powered by PV was introduced. The PV array, battery, pumps and power electronic converters and controls were designed and simulated using *PSCADTM/EMTDCTM*, which is a tool typically employed for power system transient analysis. Protection features embedded in today's inverters such as anti-islanding was implemented in the inverter controls. In chapter 1 and 2, research background of relevant topics were reviewed and theoretical fundamentals as well as different control strategies of PV systems were introduced.

In chapter 3, a significant concept and computer implementation of a multi-megawatt PV system integrated with BESS was introduced. This PV system was

divided into several sections with each section having its own DC-DC converter for MPPT and interfaced to the grid via an inverter and transformer. To avoid circulation current within the multi-megawatt system, sections are connected to the grid via individual 2 winding transformers or 3-winding transformers to interface two sections and the grid. The BESS can be installed in a separate location since it is designed to have its own DC-AC converter, which is used to supply controlled amount of real and reactive power to the grid.

In chapter 4, a proposed design technique is used to expand the capacity of an existing irrigation farm with PMSM driven pumps energized by PV and capable of achieving capacity modulation with minimum dependence on the grid. The voltage variation concern with DC-link capacitors in conventional PV inverters is eliminated with a battery energy storage, which charges and discharges power to the DC-link through a DC-DC converter so it serves as a buffer to eliminate mismatch between the power available from the PV array and power demand from the load.

5.2 Future Work

The thesis has discussed methods for interconnection of battery energy storage integrated solar PV sources with the grid along with associated control schemes. With the increasing penetration of PV, multi-MW PV farms with a large number of PV units are becoming common. A widely used practice is to interconnect each of these units to the grid via a power frequency transformer, which performs the dual function

of galvanic isolation and voltage step-up. The power frequency transformer requires significant investment in terms of space. The recent availability of high voltage band gap devices switching at very high frequencies make it possible to replace the power frequency transformer with a high switching frequency inverter of the conventional or possibly a novel type followed by a high frequency transformer, leading to a compact system.

The effect of PV penetration on grid stability has been investigated, and it was found that with the small relative ratings of the PV system, the threat to stability is minimal. However, future studies can investigate the effect of the relative PV system size, and control strategies employed, on the stability, particularly in case of loss of power from the PV due to shading. In the systems considered, the battery energy storage system supplies the power deficit in case of shading. Optimal sizing of the battery energy storage system for reliability and system cost can be investigated. Further, in case of loss of power from both the PV and battery, an optimum strategy to identify which generating station would meet the power deficit, based on cost and reliability consideration can be developed. Another possible area of work may be to investigate the use of battery integrated PV systems as spinning reserves leading to savings in operational cost.

The use of PV-battery systems for capacity expansion of irrigation plants has been explored. Multiple variable speed machine pumps fed from a battery integrated

PV system also provided capacity modulation. A possible configuration could be to use a single MW rated variable speed pump, PM or induction, instead of multiple devices, designed to operate at a flat efficiency over a wide speed range. The design of such a machine may be an area of future work. Other problems of potential interest for future investigation may involve controlling the multiple variable speed pumps using a single inverter, and other system configurations, meeting the objectives of speed control, and maximum power point tracking with a minimum number power electronics interfaces.

References

- [1] “Solrenview.” [Online]. Available: <https://www.solrenview.com/SolrenView/mainFr.php?siteId=3428>
- [2] “Photovoltaic systems,” Jul 2013. [Online]. Available: <http://yourhome.gov.au/energy/photovoltaic-systems>
- [3] “Solar cell I-V characteristic and the solar cell I-V curve.” [Online]. Available: <http://www.alternative-energy-tutorials.com/energy-articles/solar-cell-i-v-characteristic.html>
- [4] R. D. Doncker, D. W. Pulle, and V. Andre, *Advanced Electrical Drives Analysis, Modeling, Control*. Springer Netherlands, 2011.
- [5] Y. Wang, D. M. Ionel, M. Jiang, and S. Stretz, “Large scale optimization of electronically controlled synchronous reluctance machines using CE-FEA and differential evolution,” in *2015 IEEE International Electric Machines Drives Conference (IEMDC)*, May 2015, pp. 1702–1708.
- [6] D. M. I. Seyed Ahmad Hamidi and A. Nasiri, *Renewable Energy Devices and Systems with Simulations in MATLAB and ANSYS*.
- [7] “IEEE 14 bus knowledge base,” <https://hvinc.ca/knowledge-base/read,article/26/ieee-14-bus-system/v;>, accessed: 2016-08-03.

- [8] A. Aruchamy, G. Aravamudan, and G. V. S. Rao, “Semiconductor based photoelectrochemical cells for solar energy conversion—an overview,” *Bulletin of Materials Science*, vol. 4, no. 5, pp. 483–526, dec 1982. [Online]. Available: <https://doi.org/10.1007/bf02824960>
- [9] D. M. Chapin, C. S. Fuller, and G. L. Pearson, “A new silicon P-N junction photocell for converting solar radiation into electrical power,” *Journal of Applied Physics*, vol. 25, no. 5, pp. 676–677, may 1954. [Online]. Available: <https://doi.org/10.1063/1.1721711>
- [10] I. E. A. P. S. Programme, “Snapshot of global photovoltaic markets,” *International Energy Agency’s Photovoltaic Power System Programme*, 2016.
- [11] D. Spiers, “Batteries in PV systems,” in *Practical Handbook of Photovoltaics*. Elsevier, 2012, pp. 721–776. [Online]. Available: <https://doi.org/10.1016/b978-0-12-385934-1.00022-2>
- [12] R. Teodorescu, M. Liserre, and P. Rodriguez, *Introduction*. Wiley-IEEE Press, 2011, pp. 1–4. [Online]. Available: <http://ieeexplore.ieee.org.ezproxy.uky.edu/xpl/articleDetails.jsp?arnumber=5732936>
- [13] N. Bosco, T. J. Silverman, and S. Kurtz, “The influence of PV module materials and design on solder joint thermal fatigue durability,” *IEEE Journal of Photovoltaics*, vol. 6, no. 6, pp. 1407–1412, Nov 2016.
- [14] T. Moriarty, R. France, and M. Steiner, “Rapid, enhanced IV characterization of multi-junction PV devices under one sun at nrel,” in *2015 IEEE 42nd Photovoltaic Specialist Conference (PVSC)*, June 2015, pp. 1–3.
- [15] P. J. Verlinden, A. Lewandowski, H. Kendall, S. Carter, K. Cheah, I. Varfolomeev, D. Watts, M. Volk, I. Thomas, P. Wakeman, A. Neumann, P. Gizinski,

- D. Modra, D. Turner, and J. B. Lasich, "Update on two-year performance of 120 kwp concentrator PV systems using multi-junction iii ;v solar cells and parabolic dish reflective optics," in *2008 33rd IEEE Photovoltaic Specialists Conference*, May 2008, pp. 1–6.
- [16] P. J. Verlinden and J. B. Lasich, "Energy rating of concentrator PV systems using multi-junction iii ;v solar cells," in *2008 33rd IEEE Photovoltaic Specialists Conference*, May 2008, pp. 1–6.
- [17] L. E. Chaar, L. A. Lamont, and N. Elzein, "PV technology - industry update," in *IEEE PES General Meeting*, July 2010, pp. 1–6.
- [18] J. R. Finn, B. R. Hansen, and J. E. Granata, "Multiple junction cell characterization using the LBIC method: early results, issues, and pathways to improvement," in *2009 34th IEEE Photovoltaic Specialists Conference (PVSC)*, June 2009, pp. 000 564–000 569.
- [19] T. S. Babu, J. P. Ram, T. Dragicevic, M. Miyatake, F. Blaabjerg, and N. Rajasekar, "Particle swarm optimization based solar PV array reconfiguration of the maximum power extraction under partial shading conditions," *IEEE Transactions on Sustainable Energy*, vol. PP, no. 99, pp. 1–1, 2017.
- [20] S. A. O. da Silva, L. P. Sampaio, F. M. de Oliveira, and F. R. Durand, "Feed-forward DC-bus control loop applied to a single-phase grid-connected PV system operating with PSO-based mppt technique and active power-line conditioning," *IET Renewable Power Generation*, vol. 11, no. 1, pp. 183–193, 2017.
- [21] E. Malarvizhi, J. Kamala, and A. Sivasubramanian, "Evaluation of particle swarm optimization algorithm in photovoltaic applications," in *2016 10th International Conference on Intelligent Systems and Control (ISCO)*, Jan 2016, pp. 1–6.

- [22] Y. Zheng, W. Wang, W. Chen, and Q. Li, “Research on MPPT of photovoltaic system based on PSO under partial shading condition,” in *2016 35th Chinese Control Conference (CCC)*, July 2016, pp. 8654–8659.
- [23] C. K. Nayak and M. R. Nayak, “Optimal battery energy storage sizing for grid connected PV system using IHSA,” in *2016 International Conference on Signal Processing, Communication, Power and Embedded System (SCOPEs)*, Oct 2016, pp. 121–127.
- [24] T. Hou, Y. Cui, Y. Li, W. Zhang, and X. Zhou, “Sizing battery energy storage for wind farms based on wind power forecast uncertainty in the bulk power system,” in *2016 IEEE PES Asia-Pacific Power and Energy Engineering Conference (APPEEC)*, Oct 2016, pp. 1548–1552.
- [25] M. Gitizadeh and H. Fakharzadegan, “Effects of electricity tariffs on optimal battery energy storage sizing in residential PV/storage systems,” in *2013 International Conference on Energy Efficient Technologies for Sustainability*, April 2013, pp. 1072–1077.
- [26] A. I. Nikolaidis, Y. Koumparou, G. Makrides, V. Efthymiou, G. E. Georghiou, and C. A. Charalambous, “Reliable integration of a concentrating solar power plant in a small isolated system through an appropriately sized battery energy storage system,” *IET Renewable Power Generation*, vol. 10, no. 5, pp. 735–742, 2016.
- [27] A. Delavari, I. Kamwa, and A. Zabihinejad, “A comparative study of different multilevel converter topologies for battery energy storage application,” in *2017 IEEE 30th Canadian Conference on Electrical and Computer Engineering (CCECE)*, April 2017, pp. 1–5.

- [28] D. Bazargan, S. Filizadeh, and A. M. Gole, “Stability analysis of converter-connected battery energy storage systems in the grid,” *IEEE Transactions on Sustainable Energy*, vol. 5, no. 4, pp. 1204–1212, Oct 2014.
- [29] Z. Wang, H. Lin, Y. Ma, and T. Wang, “A prototype of modular multilevel converter with integrated battery energy storage,” in *2017 IEEE Applied Power Electronics Conference and Exposition (APEC)*, March 2017, pp. 434–439.
- [30] Y. C. Jeung and D. C. Lee, “Sliding mode control of bi-directional dual active bridge DC/DC converters for battery energy storage systems,” in *2017 IEEE Applied Power Electronics Conference and Exposition (APEC)*, March 2017, pp. 3385–3390.
- [31] M. Wang, F. Luo, and L. Xu, “A double-end sourced wire-bonded multi-chip SiC MOSFET power module with improved dynamic current sharing,” *IEEE Journal of Emerging and Selected Topics in Power Electronics*, vol. PP, no. 99, pp. 1–1, 2017.
- [32] K. Vechalapu, A. Negi, and S. Bhattacharya, “Comparative performance evaluation of series connected 15 kv SiC igbt devices and 15 kv SiC MOSFET devices for mv power conversion systems,” in *2016 IEEE Energy Conversion Congress and Exposition (ECCE)*, Sept 2016, pp. 1–8.
- [33] L. Wang, Y. Shi, Y. Shi, R. Xie, and H. Li, “Ground leakage current analysis and suppression in a 60 kW 5-level T-type transformerless SiC PV inverter,” *IEEE Transactions on Power Electronics*, vol. PP, no. 99, pp. 1–1, 2017.
- [34] H. Chen and D. Divan, “Soft-switching solid state transformer (S4T),” *IEEE Transactions on Power Electronics*, vol. PP, no. 99, pp. 1–1, 2017.

- [35] T. W. o. contributor, “Solar has become america’s fastest-growing, nonpartisan energy source,” Mar 2017. [Online]. Available: <http://thehill.com/blogs/pundits-blog/energy-environment/324334-solar-has-become-americas-fastest-growing-non-partisan>
- [36] R. Messenger, *Photovoltaic systems engineering*. Boca Raton, FL: CRC Press/Taylor & Francis, 2010.
- [37] T. Markvart and L. Castaner, *Solar Cells: Materials, Manufacture and Operation*. Elsevier Science, 2005. [Online]. Available: <https://www.amazon.com/Solar-Cells-Materials-Manufacture-Operation/dp/1856174573%3FSubscriptionId%3D0JYN1NVW651KCA56C102%26tag%3Dtechkie-20%26linkCode%3Dxm2%26camp%3D2025%26creative%3D165953%26creativeASIN%3D1856174573>
- [38] S. Vemuru, P. Singh, and M. Niamat, “Modeling impact of bypass diodes on photovoltaic cell performance under partial shading,” in *2012 IEEE International Conference on Electro/Information Technology*, May 2012, pp. 1–5.
- [39] A. Yafaoui., B. Wu, and R. Cheung, “Implementation of maximum power point tracking algorithm for residential photovoltaic systems,” in *2nd Canadian Solar Buildings Conference*, June 2007.
- [40] D. P. Hohm and M. E. Ropp, “Comparative study of maximum power point tracking algorithms using an experimental, programmable, maximum power point tracking test bed,” in *Photovoltaic Specialists Conference, 2000. Conference Record of the Twenty-Eighth IEEE*, 2000, pp. 1699–1702.
- [41] A. Safari and S. Mekhilef, “Simulation and hardware implementation of incremental conductance MPPT with direct control method using Cuk converter,”

- IEEE Transactions on Industrial Electronics*, vol. 58, no. 4, pp. 1154–1161, April 2011.
- [42] E. S.-T. Importados), *Power Electronics Handbook - 3 Ed.* Elsevier (St-Tecnico Importados), 2011.
- [43] K. K. H. Dia, Ahammad, S. Islam, and M. A. Choudhury, “A single phase input switched sepic pfc ac-dc converter,” in *2016 3rd International Conference on Electrical Engineering and Information Communication Technology (ICEEICT)*, Sept 2016, pp. 1–6.
- [44] Y. Ding, Y. Li, C. Liu, and Z. Sun, “Chapter 2 - solar electrical energy storage,” in *Solar Energy Storage*, B. Srensen, Ed. Boston: Academic Press, 2015, pp. 7 – 25. [Online]. Available: <http://www.sciencedirect.com/science/article/pii/B9780124095403000025>
- [45] D. Hart and K. Birson, “Deployment of solar photovoltaic generation capacity in the united states,” *journaltitle*, 2016. [Online]. Available: <https://energy.gov/sites/prod/files/2017/01/f34/Deployment%20of%20Solar%20Photovoltaic%20Generation%20Capacity%20in%20the%20United%20States.pdf>
- [46] W. Wu, N. Pongratananukul, W. Qiu, K. Rustom, T. Kasparis, and I. Batarseh, “Dsp-based multiple peak power tracking for expandable power system,” in *Applied Power Electronics Conference and Exposition, 2003. APEC '03. Eighteenth Annual IEEE*, vol. 1, Feb 2003, pp. 525–530 vol.1.
- [47] T. Noguchi, S. Togashi, and R. Nakamoto, “Short-current pulse-based maximum-power-point tracking method for multiple photovoltaic-and-converter module system,” *IEEE Transactions on Industrial Electronics*, vol. 49, no. 1, pp. 217–223, Feb 2002.

- [48] T. L. Kottas, Y. S. Boutalis, and A. D. Karlis, “New maximum power point tracker for PV arrays using fuzzy controller in close cooperation with fuzzy cognitive networks,” *IEEE Transactions on Energy Conversion*, vol. 21, no. 3, pp. 793–803, Sept 2006.
- [49] A. Kalbat, “Pscad simulation of grid-tied photovoltaic systems and total harmonic distortion analysis,” in *Electric Power and Energy Conversion Systems (EPECS), 2013 3rd International Conference on*, Oct 2013, pp. 1–6.
- [50] V. Vekhande and B. G. Fernandes, “Module integrated dc-dc converter for integration of photovoltaic source with DC micro-grid,” in *IECON 2012 - 38th Annual Conference on IEEE Industrial Electronics Society*, Oct 2012, pp. 5657–5662.
- [51] B. M. T. Ho, S. H. Chung, and S. Y. R. Hui, “An integrated inverter with maximum power tracking for grid-connected PV systems,” in *Applied Power Electronics Conference and Exposition, 2004. APEC '04. Nineteenth Annual IEEE*, vol. 3, 2004, pp. 1559–1565 Vol.3.
- [52] S. Essakiappan, H. S. Krishnamoorthy, P. Enjeti, R. S. Balog, and S. Ahmed, “Multilevel medium-frequency link inverter for utility scale photovoltaic integration,” *IEEE Transactions on Power Electronics*, vol. 30, no. 7, pp. 3674–3684, July 2015.
- [53] S. Jain and V. Agarwal, “A single-stage grid connected inverter topology for solar PV systems with maximum power point tracking,” *IEEE Transactions on Power Electronics*, vol. 22, no. 5, pp. 1928–1940, Sept 2007.
- [54] V. Vekhande, N. Kothari, and B. G. Fernandes, “Switching state vector selection strategies for paralleled multilevel current-fed inverter under unequal DC-link

- currents condition,” *IEEE Transactions on Power Electronics*, vol. 30, no. 4, pp. 1998–2009, April 2015.
- [55] G. Velasco-Quesada, F. Guinjoan-Gispert, R. Pique-Lopez, M. Roman-Lumbreras, and A. Conesa-Roca, “Electrical PV array reconfiguration strategy for energy extraction improvement in grid-connected PV systems,” *IEEE Transactions on Industrial Electronics*, vol. 56, no. 11, pp. 4319–4331, Nov 2009.
- [56] J. H. R. Enslin, M. S. Wolf, D. B. Snyman, and W. Swiegers, “Integrated photovoltaic maximum power point tracking converter,” *IEEE Transactions on Industrial Electronics*, vol. 44, no. 6, pp. 769–773, Dec 1997.
- [57] G. R. Walker and P. C. Sernia, “Cascaded DC-DC converter connection of photovoltaic modules,” *IEEE Transactions on Power Electronics*, vol. 19, no. 4, pp. 1130–1139, July 2004.
- [58] Y. Yang and F. Blaabjerg, “Overview of single-phase grid-connected photovoltaic systems,” *Electric Power Components and Systems*, vol. 43, no. 12, pp. 1352–1363, 2015.
- [59] S.-K. Kim, J.-H. Jeon, C.-H. Cho, E.-S. Kim, and J.-B. Ahn, “Modeling and simulation of a grid-connected {PV} generation system for electromagnetic transient analysis,” *Solar Energy*, vol. 83, no. 5, pp. 664 – 678, 2009.
- [60] I. H. Mahammed, Y. Bakelli, S. H. Oudjana, A. H. Arab, and S. Berrah, “Optimal model selection for PV module modeling,” in *2012 24th International Conference on Microelectronics (ICM)*, Dec 2012, pp. 1–4.
- [61] K. A. Corzine, S. D. Sudhoff, and C. A. Whitcomb, “Performance characteristics of a cascaded two-level converter,” *IEEE Transactions on Energy Conversion*, vol. 14, no. 3, pp. 433–439, Sep 1999.

- [62] E. Cengelci, S. U. Sulistijo, B. O. Woo, P. Enjeti, R. Teoderescu, and F. Blaabjerg, "A new medium-voltage PWM inverter topology for adjustable-speed drives," *IEEE Transactions on Industry Applications*, vol. 35, no. 3, pp. 628–637, May 1999.
- [63] S. Zhang, Y. Mishra, G. Nourbakhsh, and G. Ledwich, "The application of bess in load shedding scheme," in *2013 Australasian Universities Power Engineering Conference (AUPEC)*, Sept 2013, pp. 1–6.
- [64] K. Sun, L. Zhang, Y. Xing, and J. M. Guerrero, "A distributed control strategy based on dc bus signaling for modular photovoltaic generation systems with battery energy storage," *IEEE Transactions on Power Electronics*, vol. 26, no. 10, pp. 3032–3045, Oct 2011.
- [65] Power systems test case archive. [Online]. Available: https://www2.ee.washington.edu/research/pstca/pf14/pg_tca14bus.htm
- [66] T. W. o. contributor, "Solar has become america's fastest-growing, nonpartisan energy source," Mar 2017. [Online]. Available: <http://thehill.com/blogs/pundits-blog/energy-environment/324334-solar-has-become-americas-fastest-growing-non-partisan>
- [67] M. A. G. de Brito, L. Galotto, L. P. Sampaio, G. d. A. e Melo, and C. A. Canesin, "Evaluation of the main MPPT techniques for photovoltaic applications," *IEEE Transactions on Industrial Electronics*, vol. 60, no. 3, pp. 1156–1167, March 2013.
- [68] B. Xiao, L. Hang, J. Mei, C. Riley, L. M. Tolbert, and B. Ozpineci, "Modular cascaded H-bridge multilevel PV inverter with distributed MPPT for grid-connected applications," *IEEE Transactions on Industry Applications*, vol. 51, no. 2, pp. 1722–1731, March 2015.

- [69] M. Killi and S. Samanta, “Modified perturb and observe MPPT algorithm for drift avoidance in photovoltaic systems,” *IEEE Transactions on Industrial Electronics*, vol. 62, no. 9, pp. 5549–5559, Sept 2015.
- [70] P. Kumar, G. Jain, and D. K. Palwalia, “Genetic algorithm based maximum power tracking in solar power generation,” in *2015 International Conference on Power and Advanced Control Engineering (ICPACE)*, Aug 2015, pp. 1–6.
- [71] S. Pandey, B. Dwivedi, and A. Tripathi, “Closed loop boost converter control of induction motor drive fed by solar cells,” in *2016 International Conference on Emerging Trends in Electrical Electronics Sustainable Energy Systems (ICE-TEESES)*, March 2016, pp. 286–291.
- [72] H. P. H. Anh and N. H. Phuc, “Implementation an adaptive fuzzy NARX controller for MPPT PV supplied DC pump motor,” in *2012 10th International Power Energy Conference (IPEC)*, Dec 2012, pp. 550–555.
- [73] A. Bhattacharjee, D. K. Mandal, and H. Saha, “Design of an optimized battery energy storage enabled solar PV pump for rural irrigation,” in *2016 IEEE 1st International Conference on Power Electronics, Intelligent Control and Energy Systems (ICPEICES)*, July 2016, pp. 1–6.
- [74] W. Wareesri and S. Po-Ngam, “A three-phase PV-pump inverter with maximum power point tracking (MPPT) controller,” in *2016 13th International Conference on Electrical Engineering/Electronics, Computer, Telecommunications and Information Technology (ECTI-CON)*, June 2016, pp. 1–4.
- [75] E. Hayakwong, V. Kinnares, and C. Bunlaksananusorn, “Two-phase induction motor drive improvement for PV water pumping system,” in *2016 19th International Conference on Electrical Machines and Systems (ICEMS)*, Nov 2016, pp. 1–6.

- [76] S. Jain, A. K. Thopukara, R. Karampuri, and V. T. Somasekhar, “A single-stage photovoltaic system for a dual-inverter-fed open-end winding induction motor drive for pumping applications,” *IEEE Transactions on Power Electronics*, vol. 30, no. 9, pp. 4809–4818, Sept 2015.
- [77] S. Jain, R. Karampuri, and V. T. Somasekhar, “An integrated control algorithm for a single-stage PV pumping system using an open-end winding induction motor,” *IEEE Transactions on Industrial Electronics*, vol. 63, no. 2, pp. 956–965, Feb 2016.
- [78] P. Kumar, A. Gupta, R. K. Pachauri, and Y. K. Chauhan, “Utilization of energy sources in hybrid PV/FC power assisted water pumping system,” in *2015 IEEE International Conference on Computational Intelligence Communication Technology*, Feb 2015, pp. 548–553.
- [79] D. Semenov, Q. T. An, L. Sun, and G. Mirzaeva, “Nonlinear speed control for five-phase PMSM in electric vehicles,” in *2016 Australasian Universities Power Engineering Conference (AUPEC)*, Sept 2016, pp. 1–5.
- [80] Y. Cho, K. B. Lee, J. H. Song, and Y. I. Lee, “Torque-ripple minimization and fast dynamic scheme for torque predictive control of permanent-magnet synchronous motors,” *IEEE Transactions on Power Electronics*, vol. 30, no. 4, pp. 2182–2190, April 2015.
- [81] J. W. Jung, V. Q. Leu, T. D. Do, E. K. Kim, and H. H. Choi, “Adaptive PID speed control design for permanent magnet synchronous motor drives,” *IEEE Transactions on Power Electronics*, vol. 30, no. 2, pp. 900–908, Feb 2015.
- [82] M. Seilmeier and B. Piepenbreier, “Sensorless control of PMSM for the whole

- speed range using two-degree-of-freedom current control and hf test current injection for low-speed range,” *IEEE Transactions on Power Electronics*, vol. 30, no. 8, pp. 4394–4403, Aug 2015.
- [83] C. Xia, B. Ji, and Y. Yan, “Smooth speed control for low-speed high-torque permanent-magnet synchronous motor using proportional integral resonant controller,” *IEEE Transactions on Industrial Electronics*, vol. 62, no. 4, pp. 2123–2134, April 2015.
- [84] Z. Wang, J. Chen, M. Cheng, and K. T. Chau, “Field-oriented control and direct torque control for paralleled VSIs fed PMSM drives with variable switching frequencies,” *IEEE Transactions on Power Electronics*, vol. 31, no. 3, pp. 2417–2428, March 2016.
- [85] S. Ito, T. Moroi, Y. Kubo, K. Matsuse, and K. Rajashekara, “Independent control of two permanent-magnet synchronous motors fed by a four-leg inverter,” *IEEE Transactions on Industry Applications*, vol. 51, no. 1, pp. 753–760, Jan 2015.
- [86] R. Antonello, M. Carraro, A. Costabeber, F. Tinazzi, and M. Zigliotto, “Energy-efficient autonomous solar water-pumping system for permanent-magnet synchronous motors,” *IEEE Transactions on Industrial Electronics*, vol. 64, no. 1, pp. 43–51, Jan 2017.
- [87] R. Kumar and B. Singh, “Solar PV powered bldc motor drive for water pumping using Cuk converter,” *IET Electric Power Applications*, vol. 11, no. 2, pp. 222–232, 2017.
- [88] H. Lin, F. Zhao, T. A. Lipo, and B. i. Kwon, “A study on fault-tolerant operation of a two-phase permanent magnet synchronous motor based on structural

- alteration,” in *2016 IEEE Conference on Electromagnetic Field Computation (CEFC)*, Nov 2016, pp. 1–1.
- [89] G. Zhang, A. Schmidhofer, and A. Schmid, “Efficiency optimisation at DC drives for small electrical vehicles,” in *IEEE International Conference on Industrial Technology, 2003*, vol. 2, Dec 2003, pp. 1150–1155 Vol.2.
- [90] D. John and B. James, “Ac capacity modulation,” *ASHRAE Journal*, pp. 70–74, 2011.
- [91] V. Rallabandi, O. M. Akeyo, and D. M. Ionel, “Modeling of a multi-megawatt grid connected PV system with integrated batteries,” in *2016 IEEE International Conference on Renewable Energy Research and Applications (ICRERA)*, Nov 2016, pp. 1146–1151.
- [92] “Confirm solar data.” [Online]. Available: http://rredc.nrel.gov/solar/new_data/confirm/fs/

Curriculum Vitae

Oluwaseun Akeyo, Master Student

Department of Electrical and Computer Engineering, University of Kentucky

EDUCATION

Master of Science - Electrical and Computer Engineering August 2017
University of Kentucky

Thesis: Analysis and Simulation of Photovoltaic Systems
Incorporated with Battery Energy Storage
Director of Thesis: Dr. Dan M Ionel

Bachelor of Science - Electrical and Electronics Engineering May 2014
Abubakar Tafawa Balewa University, Bauchi, Nigeria

Dissertation: Design and Implementation of an Automatic
Bubble Dispenser
Advisor: Dr. Elizah Omizegba

AWARD AND RECOGNITION

2016 IEEE International Conference on Renewable Energy Research and
Applications (ICRERA) best paper award.

Nigerian Universities Engineering Students' Association (NUESA)
editor-in-chief, 2013.

EMPLOYMENT HISTORY

Research Assistant	2016.05 - Present
University of Kentucky	
Teaching Assistant	2016.01 - 2017.05
University of Kentucky	
IT support	2016.05 - 2016.08
University of Kentucky	

PUBLICATIONS

V. Rallabandi, O. M. Akeyo and D. M. Ionel, "Modeling of a multi-megawatt grid connected PV system with integrated batteries," 2016 IEEE International Conference on Renewable Energy Research and Applications (ICRERA), Birmingham, 2016, pp. 1146-1151

O. M. Akeyo, V. Rallabandi, D. M. Ionel, "Multi-Megawatt Solar PV Pumping System with Capacity Modulation and Battery Voltage Support" Submitted to 2017 IEEE International Conference on Renewable Energy Research and Applications (ICRERA), San Diego, CA.